Line-FRAP, a versatile method based on fluorescence recovery after photobleaching to measure diffusion rates *in vitro* and *in vivo*

Debabrata Dey, Shir Marciano and Gideon Schreiber

Department of Biomolecular Sciences, Weizmann Institute of Science

gideon.schreiber@weizmann.ac.il

Abstract

A cell is a densely packed conglomerate of macromolecules, where diffusion is essential for their function. The crowded conditions may affect diffusion both through hard (occluded space) and soft (weak, non-specific) interactions. Multiple-methods have been developed to measure diffusion rates at physiological protein concentrations within cells, however, each of them has its limitations. Here, we introduce Line-FRAP, a method based on measuring recovery of photobleaching under a confocal microscope that allows diffusion rate measurements for fast diffusing molecules to be measured in versatile environments using standard equipment. Implementation of Line mode to the classical FRAP technique greatly improves the time resolution in data acquisition, from 20-50 Hz in the classical mode to 800 Hz in the line mode. We also introduce an updated method for data analysis to obtain diffusion coefficients in various environments, with the number of pixels bleached at the first frame after bleaching being a critical parameter. We evaluated the method using different proteins either chemically labelled or by fusion to YFP. The calculated diffusion rates were comparable to literature data as measured *in vitro*, in HeLa cells and in *E.coli*. Diffusion coefficients in HeLa was ~2.5-fold slower and in *E.coli* 15-fold slower than measured in buffer. Moreover, we show that increasing the osmotic pressure on *E.coli* further decreases diffusion, till a point where proteins stop to move. The method presented here is easy to apply on a standard confocal microscope, fits a large range of molecules with different sizes and provides robust results in any conceivable environment and protein concentration for fast diffusing molecules.

Introduction:

For cells to function, molecules of different sizes and composition diffuse in the crowded environment to reach their targets(Dix & Verkman, 2008; Goodsell, 1991; Verkman, 2002). Fick's law, which predicts Diffusion driven by Brownian motion, is strictly valid for ideal solutions (with infinitely dilute concentrations of the solutes). It overlooks interactions between the moving species and with the surrounding (Agutter et al., 2000; Haugh, 2009; Saxton, 2012). Simulations and experiments describing molecular motions in a complex environment is a stiff challenge due to the various soft and hard interactions among the moving species(Baumann et al., 2010; Lenzi et al., 2016; Schavemaker et al., 2018). The classical theory of Stokes-Einstein regarding particle diffusion in ideal solution states that the diffusion constant of a particle *A* (D_A) is a function of its dimensions and the solution viscosity(Chandrasekhar, 1943; Einstein, 1905; Sutherland, 1905).

$$D_A = k_B T / 6\pi\eta r_A \qquad (1)$$

where η is the solvent viscosity, $k_B T$ is the product of the Boltzmann constant and the absolute temperature, r_A is the hydrodynamic radius of the diffusing particle and D_A is a measure of the mean squared displacements per unit time.(Sutherland, 1905) Interactions with other molecules that lower the mobility will be reflected by lower D_A values. Alternatively, if the motion of the molecule is increased because of the assistance from another faster moving dynamic molecule/surrounding environments, higher D_A values will be recorded. Both of these are known as anomalous diffusion(Haugh, 2009; Saxton, 2012). Accurate measurements of D_A values in the complex environment should correlate with the effective hydrodynamic radius, which takes into account the interactions the molecule is engaged in(Day & Kenworthy, 2009; He & Niemeyer, 2003; Mueller et al., 2010).

Over the years a wide range of different techniques have been developed to measure diffusion of different species inside the living cell. Most of these are fluorescent based. A comprehensive detail of different existing fluorescence based microscopy techniques and their utility/limitations are shown in supporting information, Table S1. Among them, Fluorescence recovery after Photobleaching (FRAP) (Kitamura et al., 2015; Lippincott-Schwartz et al., 2003; Phair & Misteli, 2000; Verkman, 2003), fluorescence correlation microscopy (FCS) (Bacia et al., 2006; Cluzel et al., 2000; Dauty & Verkman, 2004; Ramadurai et al., 2009) and single

particle tracking (SPT) (Manley et al., 2008) are the most popular. On the other hand, techniques like RCIS (Digman & Gratton, 2009), FSM (Waterman-Storer et al., 1998) or PIPE (Gura Sadovsky et al., 2017) are less frequently used. These techniques, separately or in combination, give reasonable diffusion values within the accepted ranges reported in the literature(Mika & Poolman, 2011; Miyawaki, 2011). Still, diffusion values reported by different research groups vary, predominantly inside the complex environment of the cell(Kingsley et al., 2018). In addition, the assumptions of different mathematical models and imposed boundary conditions on the data processing of the different techniques can influence the results, which ultimately leads to a diversified range of diffusion values(Kingsley et al., 2018). Even for a specific molecule of interest using a single instrumental technique, diversified diffusion values create confusion and misunderstanding about the model and its underlying assumptions(Kingsley et al., 2018).

FCS is considered the gold standard for calculating diffusion coefficients in solution phase. However, it requires the measured particles to be very dilute (as low as ~1 - 10 nM), and a high quantum yield of the measured particle. This imposes sever limitations for measurements in crowded environments like inside the living cell. Moreover, if molecules have some bound fraction that is immobile, FCS remains completely blind to this fraction(Ries & Schwille, 2008; Wachsmuth, 2014). In addition, FCS has limitations regarding accurate detection of slowly binding molecules(Wachsmuth, 2014).

FRAP, is the most widely used technique by experimental biologists because of the relative ease of performing confocal FRAP in the majority of the biological domains. This technique is also very sensitive towards the bound or immobile fractions of the molecules under study(Costantini & Snapp, 2013; González-González et al., 2012; Hardy, 2012; Zuleger et al., 2013). However, there are major limitation associated with the FRAP technique. For one is the relative slow data accumulation rate, making it insensitive to fast diffusing particles(Wachsmuth, 2014). Second, the conversion of FRAP rates to D_A is problematic, and requires making multiple assumptions(Angelides et al., 1988; Axelrod et al., 1976; Braga et al., 2004; Deschout et al., 2010; Kang et al., 2009; Seiffert & Oppermann, 2005; Smisdom et al., 2011; Soumpasis, 1983; Sprague et al., 2004; Waharte et al., 2010). Here, we present a modified FRAP method to calculate D_A from *in vitro* to *in vivo* and provide robust diffusion data, similar to those determined using FCS. To overcome the slow data acquisition of the confocal microscope we devised a line-FRAP method, where a single scan along a line is repeated at ~1000 Hz. The use of two simultaneous scanners reduced the dead time of the

instrument, resulting in further increase in efficiency of the line FRAP(Braeckmans et al., 2007). Careful evaluation of the size of the bleached area resulted in robust diffusion results for proteins and small molecules in varied conditions, including simple buffers, eukaryotic cells and the dense milieu of the bacterial cytoplasm under varying osmotic stresses.

Results

Theoretical background on extracting diffusing rates from FRAP data

Extracting diffusion coefficient values from FRAP recovery profiles is not straightforward(Angelides et al., 1988; Axelrod et al., 1976; Braga et al., 2004; Deschout et al., 2010; Kang et al., 2009; Seiffert & Oppermann, 2005; Smisdom et al., 2011; Soumpasis, 1983; Sprague et al., 2004; Waharte et al., 2010). The easiest way is to calculate half time of recovery ($\tau_{1/2}$) of the FRAP spot, which is defined as the time required for 50% recovery of the bleach spot(Lajoie et al., 2007; Salmon et al., 1984; Stricker et al., 2002; Zotter et al., 2017). Nevertheless, as also shown previously, $\tau_{1/2}$ measurements may actually be misleading, particularly as they do not take into account the processes occurring during bleach(Axelrod et al., 1976; Soumpasis, 1983). The classic equation derived by Soumpasis(Soumpasis, 1983) relating FRAP to the diffusion rate is:

$$Dr_n = 0.224\frac{r_n^2}{\tau_{1/2}} \quad (2)$$

This equation assumes a uniform radius of the bleach area (r_n)(Axelrod et al., 1976; Soumpasis, 1983). This relation is strictly valid for a pure isotropic diffusion model(Axelrod et al., 1976; Soumpasis, 1983). However, the main assumption i.e., diffusion during photobleaching is neglected, making its use for real FRAP experimental conditions limited. For normal laser scanning confocal microscopes, the relatively longer scanning durations increases the probability of significant amount of diffusions even during the photobleaching time pulse. This phenomenon obviously will be more common for faster diffusing molecules. Therefore, *D* values calculated from equation 2 can lead to underestimation of actual *D* in many systems(Braga et al., 2004; Kang et al., 2009; Pucadyil & Chattopadhyay, 2006; Weiss, 2004). Kang et.al. (Kang et al., 2012) solved these limitations by incorporating a new parameter, the effective bleach radius r_e. The final usable form of the modified equation is:

$$D_{confocal} = \frac{r_e^2 + r_n^2}{8\tau_{1/2}} \qquad (3)$$

When bleaching is instantaneous (i.e. for very short time pulse laser, $r_e = r_n$) $D = 0.25\frac{r_n^2}{\tau_{1/2}}$, which is similar to equation 2 (Kang et al., 2012). For the common case, where $r_e \neq r_n$ we determined experimentally r_e, r_n and $\tau_{1/2}$ in different conditions for line-FRAP, averaging 30 measurements for each sample and then using the effective bleach radius r_e in equation 3 to determine D_{confocal}.

Line FRAP methodology

Fig. 1A shows a pictorial representation of the Line-FRAP method performed in a life HeLa cell expressing CFP (Cyan Fluorescent protein), showing both the fluorescence and transmission Channels. The small red circle denotes the bleaching area, which is done by a Clip tornado (of 4-pixel size, 1 pixel length equals to 0.207 micro meter) as defined by the Olympus confocal system. The white line is the scanning line, which is performed at a rate of 800 Hz, to follow FRAP as a function of time. As we record only a line, the method is named as Line-FRAP (Braeckmans et al., 2007). Figure 1B shows the Line-FRAP cross section profile as a function of time. The vertical direction of the line denotes the time progress. The vertical red lines in the left panel shows the Region of Interest (ROI), from which the fluorescence intensity over time is plotted (Figure 1C). The horizontal rectangular area marked as 1 (red color) in Fig. 1B right panel denotes the time frame immediate after the photo-bleach pulse (the highly intense green is the bleach pulse). The time interval between each line measurement is 1.25 millisecond. The darker region reflects the bleached area. A typical example of a FRAP recovery profile (averaged over 30 individual shots) is shown in Figure 1C. The red line denotes fitting the data to a double exponential progression curve.

Several mathematical functions were tested to fit the FRAP recovery data. The bi-exponential function gave a better fit than a single exponent function, not only in complex environments but also in simple PBS buffer solution. The two-rate constant parameter k_1 and k_2 with their associated amplitudes (a_1 and a_2) were used to calculate $\tau_{1/2}$ using equation 4.

$$\frac{1}{\tau_{1/2}} = \frac{p1}{\tau(1)_{1/2}} + \frac{p2}{\tau(2)_{1/2}} \qquad (4)$$

151 Where p_1 and p_2 are the fraction amplitudes of k_1 and k_2 and $\tau(1)_{1/2}$ $\tau(2)_{1/2}$ are the respective
152 half-recovery times. The reasons we observe more than one exponent in the recovery curve is
153 the diffusive boundary between the bleached area and its surrounding (Fig. 2). This relates
154 both to dispersion of the laser light and to diffusion occurring during the bleach time.

155 **Determination of r_n and r_e of the Bleach area**

156 Equation 3 is very sensitive to r_n and r_e values, which are squared, while $\tau_{1/2}$ is not. Kang et.al
157 (Kang et al., 2012) estimated r in a slow diffusing system that allows 50 – 100 ms time lapses
158 between frames. This is not relevant for fast diffusing systems, where recovery from bleach
159 will occur within the first few frames. To obtain r_n values that are disconnected from diffusion
160 we prepared a fluorescent protein sample that forms an aggregate. The sample consisted of
161 BSA labelled with CF514 dye in PBS buffer and 30 percent (v/v) glycerol. Figure 2A shows
162 Line FRAP profiles with corresponding fluorescence recovery over time traces for this sample.
163 No FRAP were observed after photo bleach pulses of 10 ms and 63 ms. Figure 2B shows the
164 bleach radius after 10, 20 and 63 ms of bleach pulses. The red circle is the set bleach of the
165 laser (4 pixels). As seen, the size of the bleached area increases with increasing bleach times,
166 which relates to the diffraction of the laser light, with the laser power set to 100% intensity in
167 all cases(Kitamura & Kinjo, 2018). To quantify the signal, we plotted the intensity versus the
168 position along the horizontal scanning line (Figure 2 C-E). To improve the signal to noise, we
169 averaged 30 individual measurements and fitted them to a Gaussian (equation 5):

170 $$f_x = A^0 + Ae^{-\frac{(x-b)^2}{2c^2}} \quad (5)$$

171 where A^0 is the offset, A the amplitude, b the midpoint and c the width, which is related to the
172 width at half maximum (FWHM) by FWHM = $2(2\ln 2)^{1/2}c$. Figure 2 (C-E) shows the Gaussian
173 fits for post-bleach fluorescence profiles for 10, 20 and 63 ms of bleach pulses respectively.

174 Nominal radius values are assumed to be fixed for a given microscope setting and laser.
175 Not so for the effective radius r_e, which depends also on the diffusion during bleach. Therefore
176 it is mandatory to measure the effective bleach radius for each sample separately. Figure 3A
177 shows Line-FRAP progression profiles and curves of BSA labelled with CF514 in PBS buffer,
178 using 10 and 63 ms bleach pulse times. Figure 3B shows the fluorescence intensity along the
179 horizontal line (after the photo bleach in Line-FRAP mode) for a single measurement. Figure
180 3C is an average of 30 measurements and figure 3D shows a gaussian fit of these data.
181 Ambiguity remains over the percent recovery to be used for calculating r_n and r_e values. Kang

et.al used 90% fluorescence signal recovery for r_e as the diameter of the effective bleach circle (Kang et al., 2012). However, this is an arbitrary choice, and therefore we preferred to obtain this value from equation 3 by comparing FRAP diffusion rates to those obtained by FCS for the same molecule. For this purpose we chose BSA, which diffusion rate has been estimated to be 63 and 51 $\mu m^2 s^{-1}$ using light scattering(Gaigalas et al., 1992), and FCS(Krouglova et al., 2004) measurements at 25ºC. Using the fitted *c* parameter in equation 5, we found that r_n and r_e should be taken at 60% of total fluorescence signal recovery, which is equal to 1.38**c*. Accordingly, r_n values for 10, 20 and 63 ms bleach pulses calculated from the Gaussian fits are 0.745, 0.98 and 1.27 µm. These values show perfect agreement with the number of dark pixels present in the Figure 2B. Table 1 shows the parameters used to obtain diffusion rates for BSA after 10 and 63 ms bleach times. While the bleach recovery rates and r_e are very different for 10 and 63 ms bleach time(Kitamura & Kinjo, 2018), the calculated diffusion coefficient is within 10% from each other, and fit previous measurements(Gaigalas et al., 1992),(Krouglova et al., 2004). Another outcome from this calibration experiment is that the calculation procedure remained exactly the same, independent on whether 10 or 63 ms bleach time were used, despite the very large differences in all measured parameters.

Comparing Line FRAP to standard FRAP

The main advantage of Line FRAP over regular FRAP is the much improved time resolution. In the Supporting Information (Figures S1 to S3) we show FRAP data, using the same microscope setup and CF514 labelled BSA as used in Figure 3, but applying classical XY FRAP. While using Line FRAP data acquisition was at 800 Hz, using standard FRAP it was 8.5 and 17 Hz for squares of 72x72 (14.90 µm x14.90 µm) or 36x36 pixels (7.45 µm x7.45 µm) respectively (Figures S1A and B show the first frame after bleach). As can be seen, 36x36 pixels is the smallest square possible to see the boundaries of the bleach spot. In Figure S1C we show XY FRAP after 10 ms bleach pulse, which obviously results in poor bleach in the first frame (58 ms after bleach). For comparison, we show the time dependent recovery and the first frames after bleach for a 10 ms bleach pulse in Figure S1D. From Figure S1 (A-D), It is clear that Line FRAP (time frame resolution of ~1.25 ms as a line) provides far superior information compared to the existing classical FRAP techniques. In Figures S2 and S3 we show an analysis of the standard FRAP data using 63ms (Figure S2A and B) and 10 ms (Figure S2C) pulse using either a 72 (A) or 36 (B) pixel frame. For 10 ms bleach pulse only the 36 pixel frame is shown. Panel D shows for comparison the Line FRAP data for a 10 ms pulse. In the right panel we show a fit of an average of 20 acquisitions to a double-exponential equation. Figure S3 shows

215 the bleach width for the measurements shown in Figure S2, fitted to a gaussian equation. The
216 calculated $\tau_{1/2}$, r_n and r_e values as well as the diffusion coefficients are given in Table S2. All
217 the calculations were done as explained for Table 1. The calculated $\tau_{1/2}$, r_n and r_e values differed
218 between the three independent FRAP measurements using the square area method as presented
219 in Table S2, and again between later and those obtained using the Line FRAP method. The
220 square FRAP gave $D_{confocal}$ values of 29, 90 and 21 $\mu m^2 s^{-1}$, while the Line FRAP gave a value
221 of 55 for 63 ms pulse bleach and 70 for 10 ms pulse bleach. The reason for the missing accuracy
222 for the standard FRAP method is the long time it takes for the first frame to be recorded (during
223 which diffusion is occurring) and the few points to fit as $\tau_{1/2}$, due to the fast diffusion and slow
224 frame rate. Overall, this shows the advantage of the Line FRAP method over conventional
225 FRAP for fast diffusing molecules, including proteins like BSA (MW 66.5 kDa).

226 **Measuring BSA diffusion in crowded environments**

227 A rigorous test for the Line FRAP method is to retrieve diffusion rates in crowded
228 environments. PEG8000 is a synthetic polymer, popular for its use as crowder in solution
229 phase. Labelled BSA was added to 0, 5, 10, 15 and 20% (w/v) of PEG8000 in PBS buffer
230 solutions. The measurements were done after 10 and 63 ms bleach pulses. Figures 4 shows
231 FRAP recovery and post-bleach intensities for 10 ms (Figure 4A and 4B) and 63 ms (4C and
232 4D) bleach pulse durations. For r_n we used 0.745, 1.27 µm values for 10 and 63 ms bleach
233 pulses respectively. Values of r_e were calculated from Figure 4B and 4D using equation 5 as
234 detailed above. Values of $\tau_{1/2}$ were calculated using equation 4. The calculated diffusion
235 coefficients were plotted versus the relative solution viscosity (Figure 4E). The different fitted
236 parameters are provided in Table S3. As expected, the measured diffusion coefficients for BSA
237 in crowded environments showed a gradual decrease with increasing relative viscosity of the
238 PEG8000 solution(Kuttner et al., 2005). The measured diffusion values were (within the error)
239 the same, independent on whether 10 or 63 ms bleach times were used, despite the very
240 different recovery profiles. The results here show that Line-FRAP is capable for measuring
241 diffusion rates in different solutions with high reproducibility.

242 **Diffusion Coefficient Measurements *in vivo***

243 Our ultimate goal is to measure Diffusion Coefficients of proteins in the crowded milieu of the
244 cell. *In vivo* measurements introduce major technical challenges, including the variability
245 between individual living cells. Therefore, single-cell measurements should be performed in
246 sufficient numbers to estimate the diversity in terms of environments as well as sample

247 variations. Here, we used two bacterial proteins from *E.coli* origin, E-fts (PDB ID **1EFU)** and
248 baeR (PDB ID **4B09)** for our experiments. According to swiss model(Bertoni et al., 2017;
249 Waterhouse et al., 2018), E-fts and baeR are homodimers (dimer MW = 60.36 kDa and 55.2
250 kDa respectively). E-fts and baeR were labelled using two methods. One was with the CF514
251 fluorescent dye and the second by fusing the proteins to YFP (monomer MW, 26.4 kDa). We
252 have used the YFP protein variant with the A206K mutation to inhibit further oligomerization
253 of the YFP(Von Stetten et al., 2012). FRAP rates were first determined in PBS (Figure 5), from
254 which their respective diffusion coefficients were calculated as detailed above for BSA. The
255 diffusion coefficients of E-fts and baeR labelled with CF514 were 37.2 and 46 $\mu m^2 s^{-1}$
256 respectively. For the YFP fused proteins (with an estimated MW of 123 and 118 kDa) the
257 diffusion coefficients were as expected slower, 22.9 and 31.4 $\mu m^2 s^{-1}$ respectively (Table S4).

258 Next, we used these proteins to determine their diffusion coefficients in both Eukaryotic
259 and prokaryotic cells, as models for *in vivo* measurements. It is known that Eukaryotic cell
260 cytoplasm are less dense than prokaryotic cell cytoplasm, which should be reflected in the
261 diffusion coefficient(Dix & Verkman, 2008; Mika & Poolman, 2011). The 4 different proteins
262 (E-fts and baeR labelled with CF514 or fused to YFP) were microinjected inside HeLa cells
263 cytoplasm. Line-FRAP experiments were performed inside intact living cells (Figure. 6).
264 FRAP rates and r_e values were determined, from which the diffusion coefficients were
265 calculated (Table S4). As expected from the increased crowding of the cytoplasm of HeLa
266 cells, slower diffusion coefficients were determined(Dix & Verkman, 2008). For CF514
267 labelled proteins diffusion coefficients of 19.5 and 19 $\mu m^2 s^{-1}$ were determined for E-fts and
268 baeR respectively (Table S4). Diffusion coefficients of 9.0 and 12.5 $\mu m^2 s^{-1}$ were determined
269 for these proteins fused to YFP (which results in approximately doubling the MW).

270 *E.coli* bacterial cells are too small for micro-injection of proteins inside the cell(Mika
271 & Poolman, 2011). Hence, baeR-YFP and E-fts-YFP proteins were expressed in the bacterial
272 cell cytoplasm. To avoid fluorescence signal saturations, we have calibrated protein expression
273 levels using the *E.coli tuner* cells(Hartinger et al., 2010), where protein expression is tightly
274 regulated. A typical example of *E.coli* cells expressing YFP fused E-fts protein is shown in
275 Figure 7A. In Figure 7B and C FRAP recovery profiles of E-fts fused with YFP and baeR fused
276 with YFP in *E.coli* cytoplasm are shown. Figures 7D and E show the post-bleach fluorescens
277 intensity profiles, from which r_e values were calculated (Table S2). For the E-fts fused to YFP
278 D = 1.6 $\mu m^2 s^{-1}$ and for baeR fused to YFP D =0.95 $\mu m^2 s^{-1}$ were calculated (Table S4). In
279 addition, we have measured the diffusion coefficient of the YFP protein by itself in the

280 cytoplasm of *E.coli tuner* cells, resulting in a value of D = 4.6 $\mu m^2 s^{-1}$. Previously, a value of
281 7.7±2.5 $\mu m^2 s^{-1}$ was determined for GFP in *E.coli* D5Hα cells using photobleaching and photo
282 activation using conventional FRAP(Elowitz et al., 1999). It was further reported that GFP
283 diffusion rates depend on the expression level, with a value of D~ 3.6±0.7 $\mu m^2 s^{-1}$ being reported
284 at higher protein expression. Furthermore, insertion of a histidine tag during construct
285 designing resulted in D~ 4.0±2.0 $\mu m^2 s^{-1}$ (Elowitz et al., 1999). The published values indicate
286 that the Line-FRAP method predicts correctly diffusion coefficients in prokaryotic cells.
287 Moreover, the data qualities generated using Line-FRAP is less noisy than those shown in
288 previous reported FRAP measurements in *E.coli*(Elowitz et al., 1999; Kumar et al., 2010).

289 Figure 8 provides a comparison of diffusion coefficient values for E-fts and baeR in
290 different environments as determined using Line-FRAP. Figure S4 shows a comparison of (A)
291 $\tau_{1/2}$ of all corresponding diffusion processes and (B) percentage of recovery after FRAP. Fusing
292 YFP doubles their MW, and subsequently the diffusion coefficients were reduced in PBS buffer
293 solution. Both the proteins with YFP fusions showed further reduced mobility in the complex
294 environment of the HeLa cell cytoplasm. It is known that mammalian cell cytoplasm is 2-3
295 times as dense as aqueous buffer solution(Dix & Verkman, 2008; Mika & Poolman, 2011).
296 Prokaryotic cell cytoplasm are further packed, with diffusion rates being over 10-fold slower
297 than in buffer(Mika & Poolman, 2011). The fold-change in diffusion coefficients from PBS to
298 HeLa to *E.coli* is also in line with the expected reduction due to the increased viscosity(Dix &
299 Verkman, 2008; Mika & Poolman, 2011).

300 To further test the validity of our Line-FRAP method, we have carried out Diffusion
301 rate measurements in *E.coli* cells under osmotically challenging environments. It is well known
302 that at higher osmotic stress, the cell wall starts to stretch causing the cytoplasm to
303 shrink(Konopka et al., 2009; Mika et al., 2014). As a consequence of the increased crowding
304 density inside the bacterial cell cytoplasm, the mobility of proteins slows down, which is
305 reflected in lower diffusion coefficient values(Konopka et al., 2009; Mika et al., 2014;
306 Sochacki et al., 2011). Figure 9A and B show normalized FRAP recovery profiles and
307 corresponding post-bleach profiles for YFP in *E.coli* under different osmotic stress conditions.
308 Figure 9C shows a comparison of the diffusion coefficient values under different osmotic
309 conditions. Figure S4C shows a comparison of $\tau_{1/2}$ of all corresponding diffusion processes
310 and Figure S4D shows the percentage of recovery after FRAP. Increasing osmolarity was done
311 by replacing the 2TY medium to HEPES buffer plus varying concentrations of NaCl. This
312 resulted in decreasing $D_{confocal}$ values, from D = 4.6 $\mu m^2 s^{-1}$ in 2TY medium (including 85 mM

313 NaCl) to 3.2, 2.4 and 1.9 $\mu m^2 s^{-1}$ in presence of 150, 300 and 500 mM NaCl respectively (Table
314 S5). Detailed visual images of *E.Coli* cells under osmotically challenging environments are
315 provided in the supporting information Figure S5 (A-D). At very high concentration of salt
316 (1000 mM NaCl), almost no recovery of YFP protein was observed inside the *E.coli* cells
317 (Figure S5D). It suggest that addition of excess salt concentration may leads to protein
318 aggregation or formation of diffusive barriers leading to compartmentalization of YFP, which
319 contributed towards the immobility of YFP in *E.Coli*.(Van Den Bogaart et al., 2007). These
320 results confirm the power of the here presented method in challenging conditions.

321 Our data show that we have developed a universal method by which one can compare
322 diffusion coefficients measurements in different environments including *in vivo* by using
323 FRAP. This allows diffusion measurements to be done using a simple, commonly available
324 setup and applying straight forward data analysis tools. Moreover, protein-concentrations used
325 for these measurements are in the μM range, which is in line with *in vivo* protein
326 concentrations. The main advantage of the here presented method is the much faster data
327 acquisition rate, which provides exact measurements of the bleach area already 1 ms after
328 bleach, in comparison to 20-100 ms in conventional FRAP. For fast diffusion molecules,
329 including proteins, this time difference is crucial to obtain exact values of the bleach diameter
330 (which is squared in equation 3) and recovery half-times, which together provide reliable
331 diffusion coefficients. We show that using the same proteins but conventional FRAP, the
332 measurements of these parameters is vastly different (due to the slow frame rate), which results
333 in inconsistent diffusion rates for fast moving molecules. Overall, the here presented system
334 has major advantages over other methods, both in usability and versatility.
335

336 **Experimental**

337 **Materials and Methods:**

338 Dulbecco's phosphate buffered saline (PBS 1X) was purchased from Biological Industries
339 (catalog no. 02-023-1A). CF514 fluorescent labelling dye was purchased from Biotium. All
340 other reagents used are described in details in a table format (Table 2, Key resources)

341 ***Mammalian Cell culture***

342 HeLa cells were grown in 35-mm glass-bottomed dishes (MatTek Corporation) in DMEM
343 (Invitrogen) supplemented with 1x pyruvate, penicillin/streptomycin (BioLabs), and 10% fetal

344 bovine serum (Equitech-BIO. Inc.). The cells were subcultured when 80% confluence was
345 reached using trypsin-EDTA for cell detachment. $2x10^5$ HeLa cells in 2.5 ml of DMEM were
346 pipetted into glass bottomed dishes and incubated overnight. The cells were cultured in humid
347 atmosphere at 37 °C and 5% CO_2. The cells were imaged 24–30 h after the seeding process.
348 Prior to the microinjection, the medium was aspirated, and the fresh medium was supplemented
349 with 25 mM HEPES, pH 7.4.

350 ***Cloning and protein expression in E.coli***

351 Three different constructs were cloned for BaeR and Efts. BaeR or Efts fused in their N-
352 terminus to YFP (with A206K mutation that prevents self-dimerization) with a linker were
353 cloned to pET21a plasmid. The same construct was cloned to pET28-his-sumo plasmid for
354 purification. In addition, BaeR or Efts were cloned to pET28-his-sumo plasmid without YFP
355 fusion. Cloning was done by RF cloning and by using a synthesized gene of YFP A206K (Twist
356 biosciences). The YFP A206K BaeR or Efts in pET21a was transformed to Tuner™(DE3)
357 Competent Cells (Novagene) which allow adjustable levels of protein expression throughout
358 all cells in a culture. They were grown in 37°C until they reached OD_{600}= 0.6 and induced by
359 adding IPTG to a final concentration of 0.1 mM in 37°C for three hours- then stored at 4°C
360 until imaging and measuring diffusion. For higher osmotic stress conditions, the YFP expressed
361 *E.coli* bacteria cells were centrifuged, and resuspended in 10 mM HEPES buffer solution (pH
362 7.2) with different NaCl salt concentrations (150-500 mM). The incubation time in buffer
363 solutions after resuspension was varied between 30 mins to 3 hours, which had to effect on the
364 calculated diffusing rates. For protein-purification, YFP A206K BaeR or Efts in pET28-his-
365 sumo and BaeR or Efts in pET28-his-sumo plasmid were transformed to BL21 (DE3)
366 competent cells. They were grown at 37°C until they reached OD_{600}= 0.6-0.8 before adding 0.1
367 mM IPTG for protein production in 16°C overnight.

368 ***Protein Purification***

369 After overnight growth, the cells were harvested for 10 minutes at 5000 rpm and stored at -
370 20°C. The pellets were resuspended in 50 mM Tris-HCl, 200 mM NaCl and 10 mM Imidazole
371 pH=8 buffer. Protease inhibitor, lysozyme and benzonase were added. After homogenization,
372 sonication was done by using 3 cycles of 10 seconds on and 30 seconds off keeping the sample
373 on ice. Then, the samples were centrifuged at 14000 rpm for 60 minutes at 4°C. The supernatant
374 was used for further purification. Ni-NTA gravity columns of 200 ul Ni-NTA (Merck) were
375 equilibrated with binding buffer containing 50 mM Tris-HCl pH=8, 200 mM NaCl, 10 mM

376 Imidazole and 10% glycerol. The supernatant was loaded onto the column after 0.45 nm
377 filtration (Millex-HV; Millipore), then, washed with 50 mM Tris-HCl, 200 mM NaCl, 20 mM
378 Imidazole and 10% glycerol twice. On column cleavage was done by sumo-protease in elution
379 buffer: 50 mM Tris-HCl, 200 mM NaCl, 10% glycerol, 1mM DTT, 1:200 sumo protease. The
380 cleavage was done one hour in room temp and then overnight at 4°C under constant rotation.
381 Elution from beads was done twice using the cleavage buffer. For BaeR and Efts this was
382 followed by anion exchange of a FF Q column (GE). Purified proteins were analyzed by SDS-
383 PAGE gel-electrophoresis and its concentrations were determined using a nanodrop. The
384 purified protein was dialyzed using midi-gebaflex 3.5 kDa (Geba) against 0.1M $NaHCO_3$
385 buffer that is compatible to labelling with CF514 dye. The protein was then aliquoted, flash-
386 frozen in liquid nitrogen, and stored at -80°C.

387 ***Protein labelling with CF514***

388 The purified BaeR and Efts were labelled with CF514 dye (Biotium) according to the
389 manufacturer recommendations. Labelled proteins were dialyzed against PBS using Gebaflex
390 3.5KDa (GeBa) and further purified from the dye using Pierce™ Dye Removal Columns
391 (Cat#22858, Thermo-Fisher scientific).

392 ***Microinjection into HeLa cells***

393 Microinjections were performed using Eppendorf FemtoJet microinjector attached to
394 Eppendorf InjectMan NI2 micromanipulator. The different fluorescent proteins were dissolved
395 in PBS and injected into cells using glass capillaries from Warner instruments and pulled by
396 vertical puller (Narishige). For every measurement, a single pressure pulse was applied to
397 deliver the sample into the cell. Air was administrated at 15– 25 hPa for 0.1-0.3 s. For
398 injections, single cells containing morphologically healthy and well-connected HeLa cells were
399 selected. Before and after the microinjection, cell morphology and the membrane integrity were
400 confirmed by visually inspecting the injected cells.

401 ***Confocal microscopy and FRAP Analysis:***

402 *Confocal microscopy.* Imaged were collected with an Olympus IX81 FluoView FV1000
403 Spectral/SIM Scanner confocal laser-scanning microscope, using 60X DIC oil-immersion
404 objective, N.A. 1.35. For CF514/YFP fluorescence measurements, excitation was done at 515-
405 nm, using a diode laser at an output power of 3% and 1% for low and high YFP/CF514 dye
406 concentrations. Emission was recorded from 530 to 630 nm using the spectral detection system.

All image analyses were performed using FluoView software and data analyses were performed using Kaleidagraph software version 4.1 (Synergy).

Line-FRAP

Line-FRAP was carried out in liquid drops, HeLa cells or *E.coli*. The target cells were imaged with the main scanner at 515-nm excitation using 3% of the maximal intensity applying a 60x differential interference contrast oil-immersion objective lens. For photobleaching, a "tornado" of 4 pixels diameter was used in the simultaneous stimulus scanner. The circle area of the bleach was kept exactly in the middle of the scanning line. The unidirectional lines were scanned with time intervals of 1.256 ms 1000 times (equivalent to 1.256 s). The number of scans before, during, and after photobleaching was 10, 42, and 948, respectively. Photobleaching was achieved with the simultaneous laser at 405-nm excitation for 10 or 63 milisecond duration, using full intensity. The simultaneous scanner moved at a speed of 100 µs/pixel to perform an efficient photobleach. We have used two simultaneous scanners during the FRAP experiments: one scanner (at 405 nm) for photobleaching and another scanner (at 515 nm) for data acquisition. We have varied the intensity of the lasers to achieve good signal/noise ratio. Fluorescence recovery plots were fitted to a double exponent growth curve. To do a comparative study, FRAP experiments were also performed inside the PBS buffer drops putting a cover slip upside like in a sandwich mode.

ACKNOWLEDGMENT

We would like to thanks Dr. Hagen Hofmann from the department of structural biology, Weizmann Institute of Science for advice and critically reading the manuscript, and Dr. Vladimir Kiss from the department of biomolecular sciences for his help in the microscopy work. The work was supported by a grant of the Israel Science Foundation number 1268/18 and a grant by the United States - Israel Binational Science Foundation number 2015376.

REFERENCES:

1. Goodsell, D. S. (1991). Inside a living cell. *Trends in Biochemical Sciences*, *16*(C), 203–206. https://doi.org/10.1016/0968-0004(91)90083-8

2. Verkman, A. S. (2002). Solute and macromolecule diffusion in cellular aqueous compartments. In *Trends in Biochemical Sciences* (Vol. 27, Issue 1, pp. 27–33). https://doi.org/10.1016/S0968-0004(01)02003-5
3. Dix, J. A., & Verkman, A. S. (2008). Crowding Effects on Diffusion in Solutions and Cells. *Annual Review of Biophysics*, *37*(1), 247–263. https://doi.org/10.1146/annurev.biophys.37.032807.125824
4. Agutter, P. S., Malone, P. C., & Wheatley, D. N. (2000). Diffusion theory in biology: A relic of mechanistic materialism. *Journal of the History of Biology*, *33*(1), 71–111. https://doi.org/10.1023/A:1004745516972
5. Haugh, J. M. (2009). Analysis of reaction-diffusion systems with anomalous subdiffusion. *Biophysical Journal*, *97*(2), 435–442. https://doi.org/10.1016/j.bpj.2009.05.014
6. Saxton, M. J. (2012). Wanted: A positive control for anomalous subdiffusion. In *Biophysical Journal* (Vol. 103, Issue 12, pp. 2411–2422). https://doi.org/10.1016/j.bpj.2012.10.038
7. Baumann, G., F. Place, R., & Foldes-Papp, Z. (2010). Meaningful Interpretation of Subdiffusive Measurements in Living Cells (Crowded Environment) by Fluorescence Fluctuation Microscopy. *Current Pharmaceutical Biotechnology*, *11*(5), 527–543. https://doi.org/10.2174/138920110791591454
8. Lenzi, E. K., Ribeiro, H. V., Tateishi, A. A., Zola, R. S., & Evangelista, L. R. (2016). Anomalous diffusion and transport in heterogeneous systems separated by a membrane. *Proceedings of the Royal Society A: Mathematical, Physical and Engineering Sciences*, *472*(2195). https://doi.org/10.1098/rspa.2016.0502
9. Schavemaker, P. E., Boersma, A. J., & Poolman, B. (2018). How important is protein diffusion in prokaryotes? In *Frontiers in Molecular Biosciences* (Vol. 5, Issue NOV). https://doi.org/10.3389/fmolb.2018.00093
10. Einstein, A. (1905). on the Movement of Small Particles Suspended in a Stationary Liquid Demanded By the Molecular- Kinetic Theory of Heat. *Annalen Der Physik*, *322*(8), 549–560. https://doi.org/10.1002/andp.19053220806
11. Sutherland, W. (1905). LXXV. A dynamical theory of diffusion for non-electrolytes and the molecular mass of albumin . *The London, Edinburgh, and Dublin Philosophical Magazine and Journal of Science*, *9*(54), 781–785. https://doi.org/10.1080/14786440509463331
12. Chandrasekhar, S. (1943). Stochastic problems in physics and astronomy. *Reviews of Modern Physics*, *15*(1), 1–89. https://doi.org/10.1103/RevModPhys.15.1
13. Mueller, F., Mazza, D., Stasevich, T. J., & McNally, J. G. (2010). FRAP and kinetic modeling in the analysis of nuclear protein dynamics: What do we really know? In *Current Opinion in Cell Biology* (Vol. 22, Issue 3, pp. 403–411). https://doi.org/10.1016/j.ceb.2010.03.002
14. Day, C. A., & Kenworthy, A. K. (2009). Tracking microdomain dynamics in cell membranes. In *Biochimica et Biophysica Acta - Biomembranes* (Vol. 1788, Issue 1, pp. 245–253). https://doi.org/10.1016/j.bbamem.2008.10.024
15. He, L., & Niemeyer, B. (2003). A novel correlation for protein diffusion coefficients based on molecular weight and radius of gyration. *Biotechnology Progress*, *19*(2), 544–548. https://doi.org/10.1021/bp0256059
16. He, L., & Niemeyer, B. (2003). A novel correlation for protein diffusion coefficients based on molecular weight and radius of gyration. *Biotechnology Progress*, *19*(2), 544–548. https://doi.org/10.1021/bp0256059

17. Verkman, A. S. (2003). Diffusion in cells measured by fluorescence recovery after photobleaching. *Methods in Enzymology*, *360*, 635–648. https://doi.org/10.1016/S0076-6879(03)60132-1
18. Lippincott-Schwartz, J., Altan-Bonnet, N., & Patterson, G. H. (2003). Photobleaching and photoactivation: Following protein dynamics in living cells. In *Nature Reviews Molecular Cell Biology* (Vol. 4, Issue SUPPL.).
19. Kitamura, A., Nakayama, Y., & Kinjo, M. (2015). Efficient and dynamic nuclear localization of green fluorescent protein via RNA binding. *Biochemical and Biophysical Research Communications*, *463*(3), 401–406. https://doi.org/10.1016/j.bbrc.2015.05.084
20. Bacia, K., Kim, S. A., & Schwille, P. (2006). Fluorescence cross-correlation spectroscopy in living cells. *Nature Methods*, *3*(2), 83–89. https://doi.org/10.1038/nmeth822
21. Dauty, E., & Verkman, A. S. (2004). Molecular crowding reduces to a similar extent the diffusion of small solutes and macromolecules: Measurement by fluorescence correlation spectroscopy. *Journal of Molecular Recognition*, *17*(5), 441–447. https://doi.org/10.1002/jmr.709
22. Ramadurai, S., Holt, A., Krasnikov, V., Van Den Bogaart, G., Killian, J. A., & Poolman, B. (2009). Lateral diffusion of membrane proteins. *Journal of the American Chemical Society*, *131*(35), 12650–12656. https://doi.org/10.1021/ja902853g
23. Cluzel, P., Surette, M., & Leibler, S. (2000). An ultrasensitive bacterial motor revealed by monitoring signaling proteins in single cells. *Science*, *287*(5458), 1652–1655. https://doi.org/10.1126/science.287.5458.1652
24. Manley, S., Gillette, J. M., Patterson, G. H., Shroff, H., Hess, H. F., Betzig, E., & Lippincott-Schwartz, J. (2008). High-density mapping of single-molecule trajectories with photoactivated localization microscopy. *Nature Methods*, *5*(2), 155–157. https://doi.org/10.1038/nmeth.1176
25. Digman, M. A., & Gratton, E. (2009). Analysis of diffusion and binding in cells using the RICS approach. *Microscopy Research and Technique*, *72*(4), 323–332. https://doi.org/10.1002/jemt.20655
26. Waterman-Storer, C. M., Desai, A., Bulinski, J. C., & Salmon, E. D. (1998). Fluorescent speckle microscopy, a method to visualize the dynamics of protein assemblies in living cells. Current Biology, 8(22), 1227–1230. https://doi.org/10.1016/s0960-9822(07)00515-5
27. Gura Sadovsky, R., Brielle, S., Kaganovich, D., & England, J. L. (2017). Measurement of Rapid Protein Diffusion in the Cytoplasm by Photo-Converted Intensity Profile Expansion. Cell Reports, 18(11), 2795–2806. https://doi.org/10.1016/j.celrep.2017.02.063
28. Mika, J. T., & Poolman, B. (2011). Macromolecule diffusion and confinement in prokaryotic cells. In *Current Opinion in Biotechnology* (Vol. 22, Issue 1, pp. 117–126). https://doi.org/10.1016/j.copbio.2010.09.009
29. Miyawaki, A. (2011). Proteins on the move: Insights gained from fluorescent protein technologies. In *Nature Reviews Molecular Cell Biology* (Vol. 12, Issue 10, pp. 656–668). https://doi.org/10.1038/nrm3199
30. Kingsley, J. L., Bibeau, J. P., Mousavi, S. I., Unsal, C., Chen, Z., Huang, X., Vidali, L., & Tuzel, E. (2018). Understanding Boundary Effects and Confocal Optics Enables Quantitative FRAP Analysis in the Confined Geometries of Animal, Plant and Fungal Cells. *Biophysical Journal*, *114*(3), 349a-350a. https://doi.org/10.1016/j.bpj.2017.11.1948

31. Ries, J., & Schwille, P. (2008). New concepts for fluorescence correlation spectroscopy on membranes. In *Physical Chemistry Chemical Physics* (Vol. 10, Issue 24, pp. 3487–3497). https://doi.org/10.1039/b718132a
32. Wachsmuth, M. (2014). Molecular diffusion and binding analyzed with FRAP. In *Protoplasma* (Vol. 251, Issue 2, pp. 373–382). https://doi.org/10.1007/s00709-013-0604-x
33. González-González, I. M., Jaskolski, F., Goldberg, Y., Ashby, M. C., & Henley, J. M. (2012). Measuring membrane protein dynamics in neurons using fluorescence recovery after photobleach. In *Methods in Enzymology* (Vol. 504, pp. 127–146). https://doi.org/10.1016/B978-0-12-391857-4.00006-9
34. Hardy, L. R. (2012). Fluorescence recovery after photobleaching (FRAP) with a focus on F-actin. *Current Protocols in Neuroscience*, *SUPPL.61*. https://doi.org/10.1002/0471142301.ns0217s61
35. Costantini, L., & Snapp, E. (2013). Probing endoplasmic reticulum dynamics using fluorescence imaging and photobleaching techniques. *Current Protocols in Cell Biology*, *SUPPL.60*. https://doi.org/10.1002/0471143030.cb2107s60
36. Zuleger, N., Kelly, D. A., & Schirmer, E. C. (2013). Considering discrete protein pools when measuring the dynamics of nuclear membrane proteins. *Methods in Molecular Biology*, *1042*, 275–298. https://doi.org/10.1007/978-1-62703-526_2
37. Axelrod, D., Koppel, D. E., Schlessinger, J., Elson, E., & Webb, W. W. (1976). Mobility measurement by analysis of fluorescence photobleaching recovery kinetics. *Biophysical Journal*, *16*(9), 1055–1069. https://doi.org/10.1016/S0006-3495(76)85755-4
38. Soumpasis, D. M. (1983). Theoretical analysis of fluorescence photobleaching recovery experiments. *Biophysical Journal*, *41*(1), 95–97. https://doi.org/10.1016/S0006-3495(83)84410-5
39. Kang, M., Day, C. A., Drake, K., Kenworthy, A. K., & DiBenedetto, E. (2009). A generalization of theory for two-dimensional fluorescence recovery after photobleaching applicable to confocal laser scanning microscopes. *Biophysical Journal*, *97*(5), 1501–1511. https://doi.org/10.1016/j.bpj.2009.06.017
40. Braga, J., Desterro, J. M. P., & Carmo-Fonseca, M. (2004). Intracellular macromolecular mobility measured by fluorescence recovery after photobleaching with confocal laser scanning microscopes. *Molecular Biology of the Cell*, *15*(10), 4749–4760. https://doi.org/10.1091/mbc.E04-06-0496
41. Angelides, K. J., Elmer, L. W., Loftus, D., & Elson, E. (1988). Distribution and lateral mobility of voltage-dependent sodium channels in neurons. *Journal of Cell Biology*, *106*(6), 1911–1925. https://doi.org/10.1083/jcb.106.6.1911
42. Seiffert, S., & Oppermann, W. (2005). Systematic evaluation of FRAP experiments performed in a confocal laser scanning microscope. *Journal of Microscopy*, *220*(1), 20–30. https://doi.org/10.1111/j.1365-2818.2005.01512.x
43. Sprague, B. L., Pego, R. L., Stavreva, D. A., & McNally, J. G. (2004). Analysis of binding reactions by fluorescence recovery after photobleaching. *Biophysical Journal*, *86*(6), 3473–3495. https://doi.org/10.1529/biophysj.103.026765
44. Deschout, H., Hagman, J., Fransson, S., Jonasson, J., Rudemo, M., Lorén, N., & Braeckmans, K. (2010). Straightforward FRAP for quantitative diffusion measurements with a laser scanning microscope. *Optics Express*, *18*(22), 22886. https://doi.org/10.1364/oe.18.022886
45. Waharte, F., Steenkeste, K., Briandet, R., & Fontaine-Aupart, M. P. (2010). Diffusion measurements inside biofilms by image-based fluorescence recovery after photobleaching (FRAP) analysis with a commercial confocal laser scanning

584 microscope. *Applied and Environmental Microbiology*, *76*(17), 5860–5869.
585 https://doi.org/10.1128/AEM.00754-10
586 46. Smisdom, N., Braeckmans, K., Deschout, H., vandeVen, M., Rigo, J.-M., De Smedt,
587 S. C., & Ameloot, M. (2011). Fluorescence recovery after photobleaching on the
588 confocal laser-scanning microscope: generalized model without restriction on the size
589 of the photobleached disk. *Journal of Biomedical Optics*, *16*(4), 046021.
590 https://doi.org/10.1117/1.3569620
591 47. Braeckmans, K., Remaut, K., Vandenbroucke, R. E., Lucas, B., De Smedt, S. C., &
592 Demeester, J. (2007). Line FRAP with the confocal laser scanning microscope for
593 diffusion measurements in small regions of 3-D samples. *Biophysical Journal*, *92*(6),
594 2172–2183. https://doi.org/10.1529/biophysj.106.099838
595 48. Stricker, J., Maddox, P., Salmon, E. D., & Erickson, H. P. (2002). Rapid assembly
596 dynamics of the Escherichia coli FtsZ-ring demonstrated by fluorescence recovery
597 after photobleaching. *Proceedings of the National Academy of Sciences of the United*
598 *States of America*, *99*(5), 3171–3175. https://doi.org/10.1073/pnas.052595099
599 49. Salmon, E. D., Leslie, R. J., Saxton, W. M., Karow, M. L., & McIntosh, J. R. (1984).
600 Spindle microtubule dynamics in sea urchin embryos: Analysis using a fluorescein-
601 labeled tubulin and measurements of fluorescence redistribution after laser
602 photobleaching. *Journal of Cell Biology*, *99*(6), 2165–2174.
603 https://doi.org/10.1083/jcb.99.6.2165
604 50. Lajoie, P., Partridge, E. A., Guay, G., Goetz, J. G., Pawling, J., Lagana, A., Bharat, J.,
605 Dennis, J. W., & Nabi, I. R. (2007). Plasma membrane domain organization regulates
606 EGFR signaling in tumor cells. *Journal of Cell Biology*, *179*(2), 341–356.
607 https://doi.org/10.1083/jcb.200611106
608 51. Zotter, A., Bäuerle, F., Dey, D., Kiss, V., & Schreiber, G. (2017). Quantifying
609 enzyme activity in living cells. *Journal of Biological Chemistry*, *292*(38), 15838–
610 15848. https://doi.org/10.1074/jbc.M117.792119
611 52. Weiss, M. (2004). Challenges and artifacts in quantitative photobleaching
612 experiments. *Traffic*, *5*(9), 662–671. https://doi.org/10.1111/j.1600-
613 0854.2004.00215.x
614 53. Pucadyil, T. J., & Chattopadhyay, A. (2006). Confocal fluorescence recovery after
615 photobleaching of green fluorescent protein in solution. *Journal of Fluorescence*,
616 *16*(1), 87–94. https://doi.org/10.1007/s10895-005-0019-y
617 54. Kang, M., Day, C. A., Kenworthy, A. K., & DiBenedetto, E. (2012). Simplified
618 equation to extract diffusion coefficients from confocal FRAP data. *Traffic*, *13*(12),
619 1589–1600. https://doi.org/10.1111/tra.12008
620 55. Kitamura, A., & Kinjo, M. (2018). Determination of diffusion coefficients in live cells
621 using fluorescence recovery after photobleaching with wide-field fluorescence
622 microscopy. *Biophysics and Physicobiology*, *15*(0), 1–7.
623 https://doi.org/10.2142/biophysico.15.0_1
624 56. Gaigalas, A. K., Hubbard, J. B., McCurley, M., & Woo, S. (1992). Diffusion of bovine
625 serum albumin in aqueous solutions. *Journal of Physical Chemistry*, *96*(5), 2355–2359.
626 https://doi.org/10.1021/j100184a063
627 57. Krouglova, T., Vercammen, J., & Engelborghs, Y. (2004). Correct diffusion
628 coefficients of proteins in fluorescence correlation spectroscopy. Application to tubulin
629 oligomers induced by Mg2+ and Paclitaxel. *Biophysical Journal*, *87*(4), 2635–2646.
630 https://doi.org/10.1529/biophysj.104.040717
631 58. Kuttner, Y. Y., Kozer, N., Segal, E., Schreiber, G., & Haran, G. (2005). Separating the
632 contribution of translational and rotational diffusion to protein association. *Journal of*

633 *the American Chemical Society*, *127*(43), 15138–15144.
634 https://doi.org/10.1021/ja053681c
635 59. Bertoni, M., Kiefer, F., Biasini, M., Bordoli, L., & Schwede, T. (2017). Modeling
636 protein quaternary structure of homo- and hetero-oligomers beyond binary interactions
637 by homology. *Scientific Reports*, *7*(1). https://doi.org/10.1038/s41598-017-09654-8
638 60. Waterhouse, A., Bertoni, M., Bienert, S., Studer, G., Tauriello, G., Gumienny, R., Heer,
639 F. T., De Beer, T. A. P., Rempfer, C., Bordoli, L., Lepore, R., & Schwede, T. (2018).
640 SWISS-MODEL: Homology modelling of protein structures and complexes. *Nucleic*
641 *Acids Research*, *46*(W1), W296–W303. https://doi.org/10.1093/nar/gky427
642 61. Von Stetten, D., Noirclerc-Savoye, M., Goedhart, J., Gadella, T. W. J., & Royant, A.
643 (2012). Structure of a fluorescent protein from Aequorea victoria bearing the obligate-
644 monomer mutation A206K. *Acta Crystallographica Section F: Structural Biology and*
645 *Crystallization Communications*, *68*(8), 878–882.
646 https://doi.org/10.1107/S1744309112028667
647 62. Hartinger, D., Heinl, S., Schwartz, H. E., Grabherr, R., Schatzmayr, G., Haltrich, D., &
648 Moll, W. D. (2010). Enhancement of solubility in Escherichia coli and purification of
649 an aminotransferase from Sphingopyxis sp. MTA144 for deamination of hydrolyzed
650 fumonisin B1. *Microbial Cell Factories*, *9*. https://doi.org/10.1186/1475-2859-9-62
651 63. Hartinger, D., Heinl, S., Schwartz, H. E., Grabherr, R., Schatzmayr, G., Haltrich, D., &
652 Moll, W. D. (2010). Enhancement of solubility in Escherichia coli and purification of
653 an aminotransferase from Sphingopyxis sp. MTA144 for deamination of hydrolyzed
654 fumonisin B1. *Microbial Cell Factories*, *9*. https://doi.org/10.1186/1475-2859-9-62
655 64. Kumar, M., Mommer, M. S., & Sourjik, V. (2010). Mobility of cytoplasmic, membrane,
656 and DNA-binding proteins in Escherichia coli. *Biophysical Journal*, *98*(4), 552–559.
657 https://doi.org/10.1016/j.bpj.2009.11.002
658 65. Mika, J. T., Schavemaker, P. E., Krasnikov, V., & Poolman, B. (2014). Impact of
659 osmotic stress on protein diffusion in Lactococcus lactis. *Molecular Microbiology*.
660 https://doi.org/10.1111/mmi.12800
661 66. Konopka, M. C., Sochacki, K. A., Bratton, B. P., Shkel, I. A., Record, M. T., &
662 Weisshaar, J. C. (2009). Cytoplasmic protein mobility in osmotically stressed
663 Escherichia coli. *Journal of Bacteriology*, *91*(1), 231–237.
664 https://doi.org/10.1128/JB.00536-08
665 67. Sochacki, K. A., Shkel, I. A., Record, M. T., & Weisshaar, J. C. (2011). Protein
666 diffusion in the periplasm of E. coli under osmotic stress. *Biophysical Journal*, *100*(1),
667 22–31. https://doi.org/10.1016/j.bpj.2010.11.044
668 68. Van Den Bogaart, G., Hermans, N., Krasnikov, V., & Poolman, B. (2007). Protein
669 mobility and diffusive barriers in Escherichia coli: Consequences of osmotic stress.
670 Molecular Microbiology, 64(3), 858–871. https://doi.org/10.1111/j.1365-
671 2958.2007.05705.x

672

673

Table 1: Diffusion Coefficients calculated from FRAP data for labeled BSA in PBS buffer at different bleach time durations

Bleach Pulse duration	k_1 ms^{-1}	k_2 ms^{-1}	a_1	a_2	p_1	p_2	τ_1	τ_2	$\tau_{1/2}$ (ave)	c_n µm	r_n µm	c_e µm	r_e µm	$D_{confocal}$ $\mu m^2 s^{-1}$
10ms	0.16	0.012	736	241	0.75	0.25	0.004	0.058	0.0056	0.54	0.74	1.15	1.59	68.5
10ms	0.16	0.013	1125	307	0.78	0.21	0.004	0.053	0.0054	0.54	0.74	1.15	1.59	71.2
63ms	0.046	0.005	726	359	0.67	0.33	0.015	0.14	0.0214	0.92	1.27	2.05	2.83	54.9
63ms	0.044	0.005	770	373	0.67	0.33	0.016	0.14	0.0222	0.92	1.27	2.05	2.83	54.2
63ms	0.046	0.005	466	254	0.65	0.35	0.015	0.13	0.0219	0.92	1.27	2.05	2.83	56.3

The rate constants (*k*) and amplitudes (a) are from the double-exponential fit of the FRAP data. The *c* values were obtained from Gaussian fits using equation 5. The respective radius (r) are calculated assuming the respective bleach circles diameter lies at 60% height from the bottom of the Gaussian Profiles (r=1.38**c*).

674

675

676

677

678

679

Table 2: Key resources

Reagent Type(Species) or resource	Designation	Source or reference	Identifiers	Additional Information
PBS buffer	Dulbecco's phosphate buffered saline (PBS 1X)	Biological Industries	Catalog no. 02-023-1A	Sterile , Tissue Culture Grade
HEPES buffer	HEPES	Fisher BioReagents	LOT 170358	Molecular Biology Grade
Labelling Dye	CF514	Biotium	CF®514 Dye Alternative green fluorescent dye	
DMEM (MEDIA)	DMEM(1X) Gibco	Biological Industries	REF#41965-039	
Fetal Bovine Serum	FBS (Gibco)	Invitrogen	REF#12657-029	
Trypsin-EDTA	Trypsin-EDTA Solution A	Biological Industries	REF#03-050-1B	
Penicillin/ Streptomycin	Pen-Strep Solution	Biological Industries	REF#03-031-1B	
Pyruvate	Sodium Pyruvate Solution	Biological Industries	REF#03-042-1B	
Glass Dishes (For cell culture)	35-mm glass-bottomed dishes	MatTek Corporation	P35G-0-14-C	Uncoated
Dye Removal Columns	Pierce™ Dye Removal Columns	Thermo-Fisher scientific	Cat#22858	
Dialysis Tube	Gebaflex tubes 3.5KDa (GeBa)	TIVAN BIOTECH	Cat#MIDI3-100	
Glass Capillaries	Capillary Glass Tubing	Warner Instruments	Model No. G120TF-4 203-776-0664	Borosilicate-Thin wall with Filament

Figure Legends:

Figure 1: (A) Line-FRAP performed in a CFP transfected HeLa cell. White line represents the scanning line; Red circular area denotes the bleaching area. (B): A single scanning line as a function of time (in vertical direction) including the bleach. The red rectangular marks the region of interest (ROI), which was used for analysis. A zoomed view of Line-FRAP profile, is also shown where horizontal rectangular area (red colored marks ROI) denotes the fluorescence intensity as a function of length across the scanning line. (C): Average of 30 FRAP recovery curves as a function of time. (N=30; Correlation coefficient R=0.98)

Figure 2: (A) Line FRAP profile of a precipitated (fixed) sample (BSA labeled with CF514 Dye in 30% Glycerol in PBS buffer) after 10 ms and 63 ms bleach pulse. Corresponding recovery profiles over time are shown. (B): Nominal bleach areas (before and after the bleach) for the precipitated samples. The green circular area marked 2, denotes the nominal bleach done by the laser when 10, 20 and 63 ms bleach pulses were used and the red circular area 1 denotes the bleach area defined by the clip tornado of 4 pixel (Inherent laser settings defined by Olympus confocal system). (C-E): Determination of nominal bleach radius (rn) from the fluorescence intensity profiles for (C) 10, (D) 20 and (E) 63 ms bleach pulse fitted using a Gaussian equation. (N=20; R=0.99 for each of the fits)

Figure 3: (A) Fluorescence recovery (FRAP) after photobleaching of BSA labelled with CF514 in PBS. Comparative data of 10 and 63 ms bleach pulse fitted to double exponential

equation are shown. (N=30; R=0.91 for 10ms and 0.97 for 63ms fit) (B-D): Determination of effective bleach sizes from the fluorescence intensity profiles for 10 and 63 ms bleach pulse. (B) Single run data, (C) average of 30 measurements. (D) Gaussian fits for the average bleach sizes after 10 and 63 ms bleach pulse. (N=30; R= 0.99 for both of the fits)

Figure 4: (A,C) FRAP recovery profiles for 10 and 63 ms bleach pulses of labeled BSA in PBS buffer in the presence of 5, 10, 15 and 20% PEG8000. (N=30 for all; R= 0.96 for 5, 0.97 for 10, 0.98 for 15 and 20% fits in A) (R= 0.98 for 5%, 0.99 for rest of the fits in C) (B, D) Average post bleach size of fluorescence intensity profiles after 10 ms (N=30 for all; R= 0.99 for each of the fits in B) and 63 ms bleach pulses fitted to a Gaussian equation. (N=30 for all; R= 0.98 for 5% and 0.99 for rest of the fits in D) (E): Diffusion Coefficients (in µm2s-1) as a function of Relative viscosity (η0 of water considered as 1, data are from panels A-D, final error bars are calculated after combining all the individual errors from the respective average fits).

Figure 5: (A-C) FRAP recovery profiles of (A) E-fts (N=25; R=0.98) (B) baeR proteins (N=30; R=0.98) labeled with CF514 dye in PBS buffer. (C) Corresponding averaged post bleach size profiles for E-fts and baeR proteins fitted to a Gaussian equation (N=100; R=0.99). (D-G): FRAP recovery profiles of (D) E-fts fused with YFP (N=30; R=0.99) (F) baeR fused with YFP (N=30; R=0.99) in PBS buffer solution. Gaussian fits of averaged post bleach size profiles for (E) E-fts fused with YFP (N=30; R=0.99) (G) baeR fused with YFP (N=30; R=0.99).

Figure 6: (A) A typical HeLa cell after successful micro-injection with a fluorescent labeled E-fts protein. (B-C): FRAP recovery profiles of (B) E-fts fused with YFP (N=43; R=0.99) (C) baeR fused with YFP (N=42; R=0.99) in HeLa cell cytoplasm. (D-E): Gaussian fits of averaged post-bleach size profiles for (D) E-fts fused with YFP (N=29; R=0.99) (E) baeR fused with YFP (N=36; R=0.99) in HeLa cell cytoplasm.

Figure 7: (A) Typical E.Coli cells after expression of YFP fused E-fts protein. (B, C): FRAP recovery profiles of (B) E-fts fused with YFP (N=49; R=0.99) (C) baeR fused with YFP (N=52; R=0.99) in E.coli cytoplasm. (D, E): Gaussian fits of post bleach size profiles for (D) E-fts fused with YFP (R= 0.98) (E) baeR fused with YFP (R= 0.97) in E.coli cytoplasm.

Figure 8: Comparing diffusion coefficients of E-fts and baeR proteins chemically labeled or fused with YFP in PBS buffer, HeLa cell cytoplasm and E.coli bacteria cells. (Final error bars are calculated after combining all the individual errors from the respective average fits).

Figure 9: (A) Normalized FRAP recovery profiles (N=20; R=0.97 for YFP in 2YT, N=30; R=0.98 in 150mM, N=30; R=0.99 in 300mM and N=30; R=0.99 in 500mM NaCl). (B) Corresponding Gaussian fits of averaged post-bleach size profiles (R=0.98 for YFP in 2YT, R=0.99 for 150mM, 300mM and 500mM NaCl). And (C) Comparison of diffusion coefficients for YFP protein expressed in E.coli cells under different osmotic stress environments (final error bars are calculated after combining all the individual errors from the respective average fits).

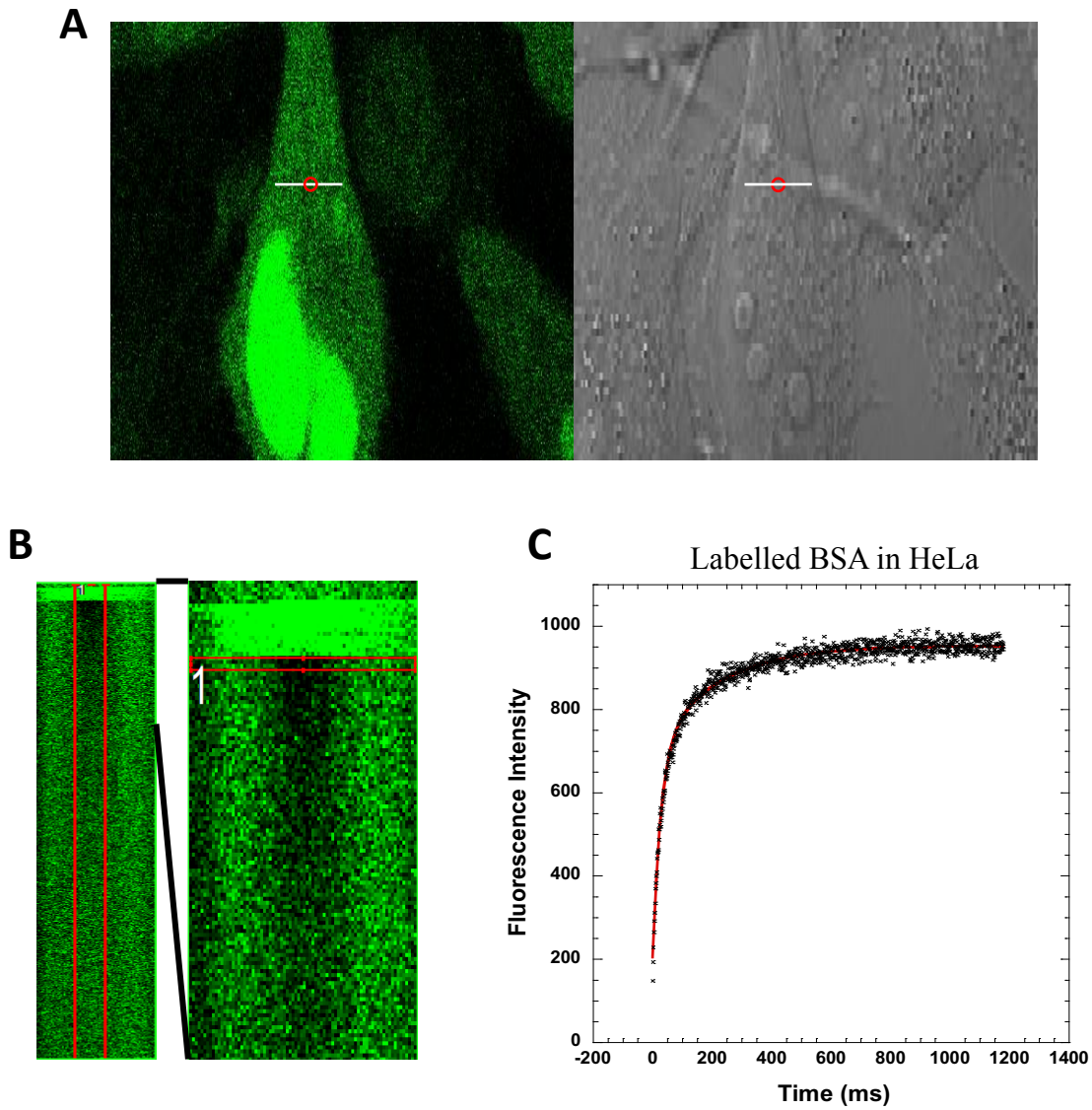

Figure 1: (A) Line-FRAP performed in a CFP transfected HeLa cell. White line represents the scanning line, Red circular area denotes the bleaching area. (B): A single scanning line as a function of time (in vertical direction) including the bleach. The red rectangular marks the region of interest (ROI), which was used for analysis. A zoomed view of Line-FRAP profile, is also shown where horizontal rectangular area (red colored marks ROI) denotes the fluorescence intensity as a function of length across the scanning line. (C): Average of 30 FRAP recovery curves as a function of time. (N=30;Correlation coefficient R=0.98)

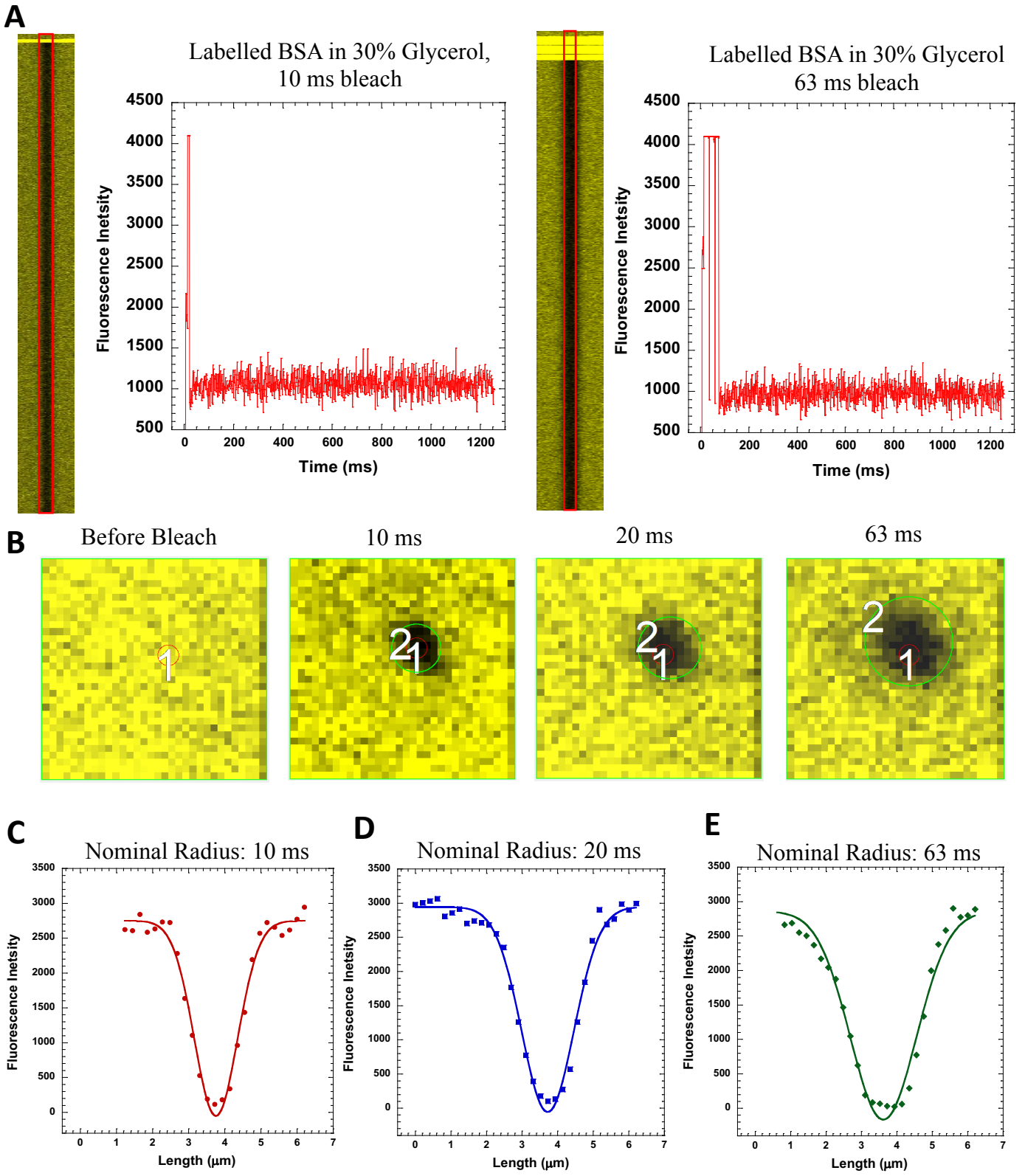

Figure 2: (A) Line FRAP profile of a precipitated (fixed) sample (BSA labeled with CF514 Dye in 30% Glycerol in PBS buffer) after 10 ms and 63 ms bleach pulse. Corresponding recovery profiles over time are shown. (B): Nominal bleach areas (before and after the bleach) for the precipitated samples. The green circular area marked 2, denotes the nominal bleach done by the laser when 10, 20 and 63 ms bleach pulses were used and the red circular area 1 denotes the bleach area defined by the clip tornado of 4 pixel (Inherent laser settings defined by Olympus confocal system). (C-E): Determination of nominal bleach radius (r_n) from the fluorescence intensity profiles for (C) 10, (D) 20 and (E) 63 ms bleach pulse fitted using a Gaussian equation. (N=20; R=0.99 for each of the fits)

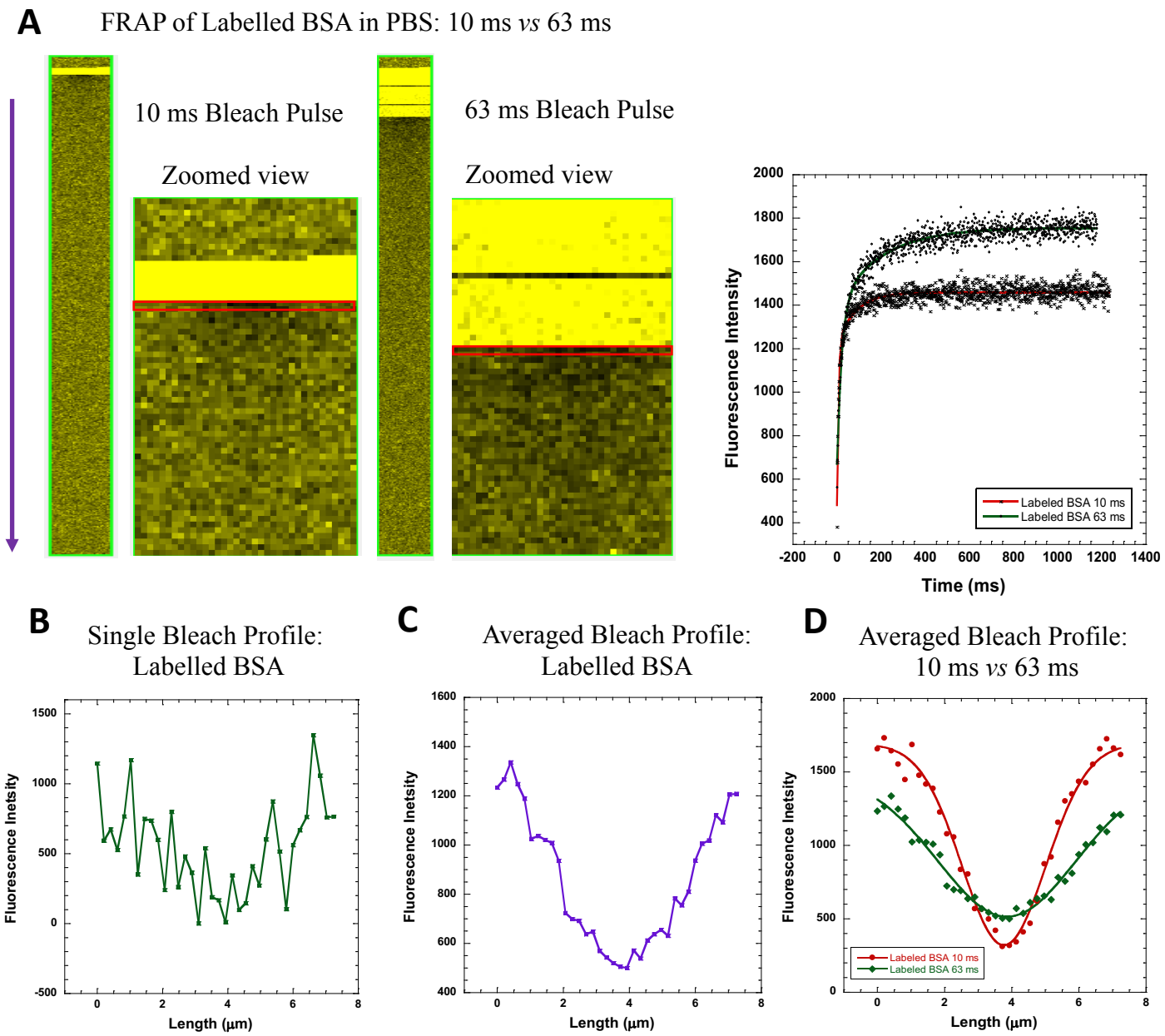

Figure 3: (A) Fluorescence recovery (FRAP) after photobleaching of BSA labelled with CF514 in PBS. Comparative data of 10 and 63 ms bleach pulse fitted to double exponential equation are shown. (N=30; R=0.91 for 10ms and 0.97 for 63ms fit) (B-D): Determination of effective bleach sizes from the fluorescence intensity profiles for 10 and 63 ms bleach pulse. (B) single run data, (C) average of 30 measurements. (D) Gaussian fits for the average bleach sizes after 10 and 63 ms bleach pulse. (N=30; R= 0.99 for both of the fits)

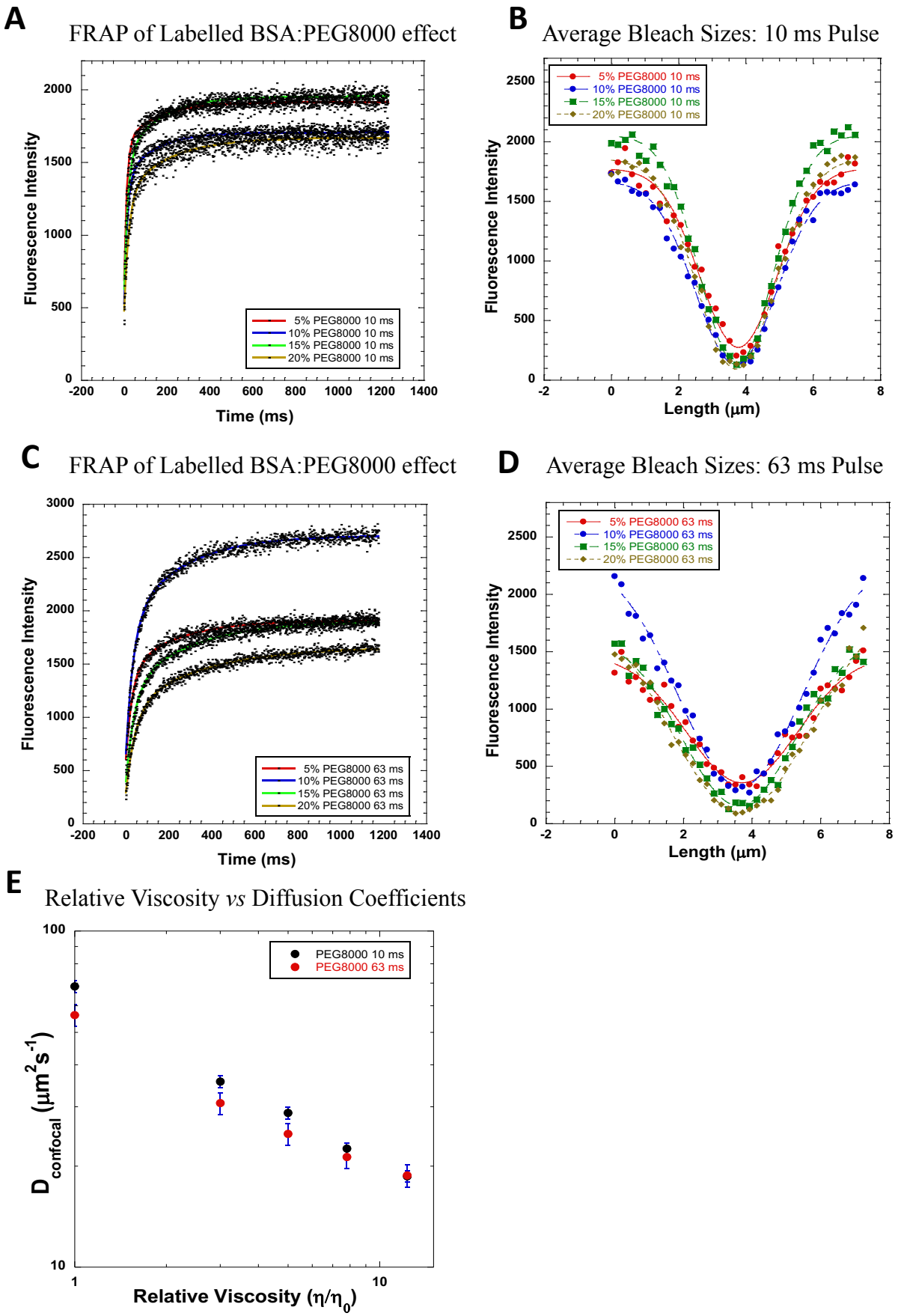

Figure 4: (A,C) FRAP recovery profiles for 10 and 63 ms bleach pulses of labeled BSA in PBS buffer in the presence of 5, 10, 15 and 20% PEG8000. (N=30 for all; R= 0.96 for 5, 0.97 for 10, 0.98 for 15 and 20% fits in A) whereas (R= 0.98 for 5%, 0.99 for rest of the fits in C) (B, D) Average post bleach size of fluorescence intensity profiles after 10 ms (N=30 for all; R= 0.99 for each of the fits in B) and 63 ms bleach pulses fitted to a Gaussian equation. (N=30 for all; R= 0.98 for 5% and 0.99 for rest of the fits in D) (E): Diffusion Coefficients (in $\mu m^2 s^{-1}$) as a function of Relative viscosity (η_0 of water considered as 1, data are from panels A-D, Final error bars are calculated after combining all the individual errors from the respective average fits).

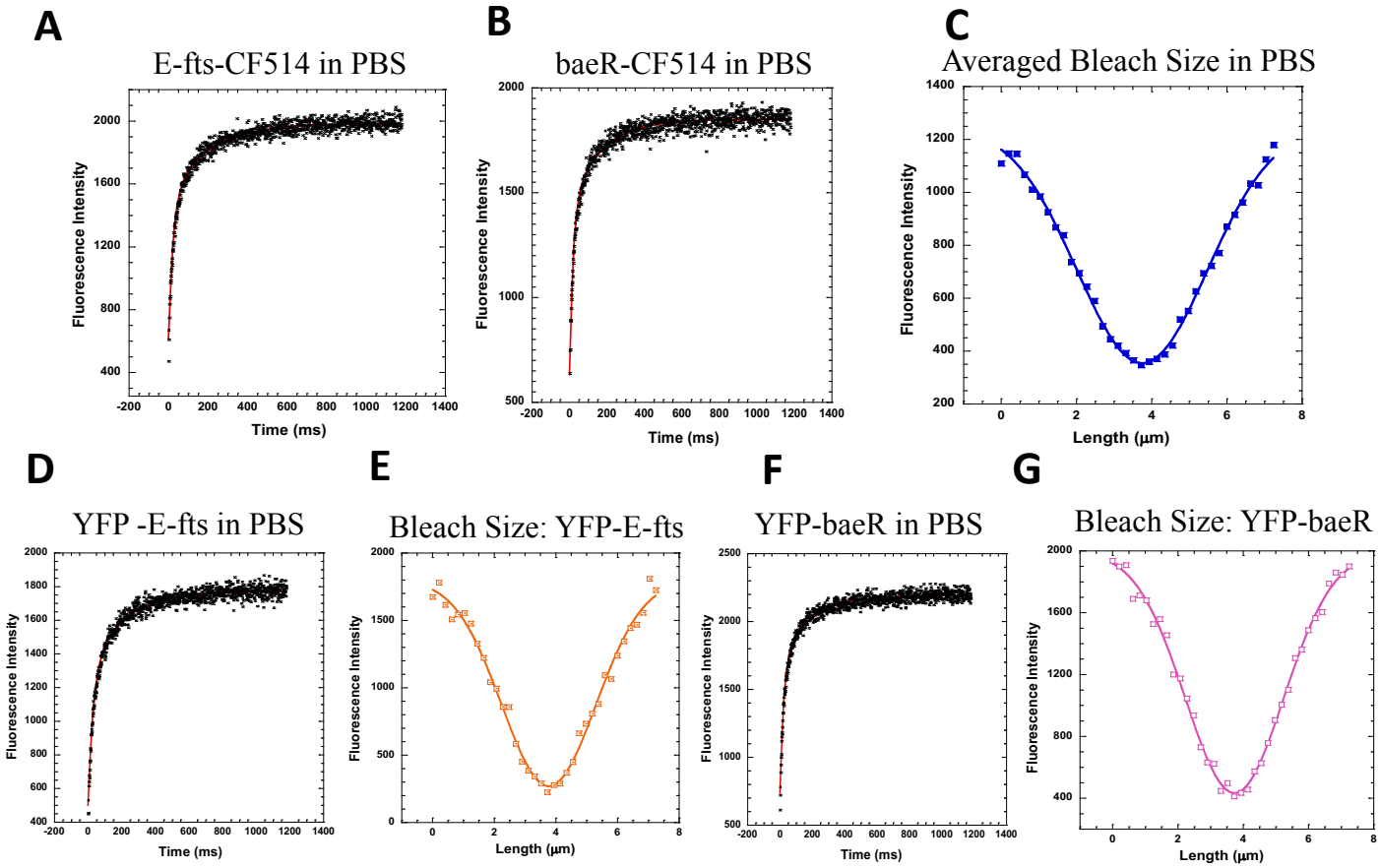

Figure 5

Figure 5: (A-C) FRAP recovery profiles of (A) E-fts (N=25; R=0.98) (B) baeR proteins (N=30; R=0.98) labeled with CF514 dye in PBS buffer. (C) Corresponding averaged post bleach size profiles for E-fts and baeR proteins fitted to a Gaussian equation (N=100; R=0.99). (D-G): FRAP recovery profiles of (D) E-fts fused with YFP (N=30; R=0.99) (F) baeR fused with YFP (N=30; R=0.99) in PBS buffer solution. Gaussian fits of averaged post bleach size profiles for (E) E-fts fused with YFP (N=30; R=0.99) (G) baeR fused with YFP (N=30; R=0.99) .

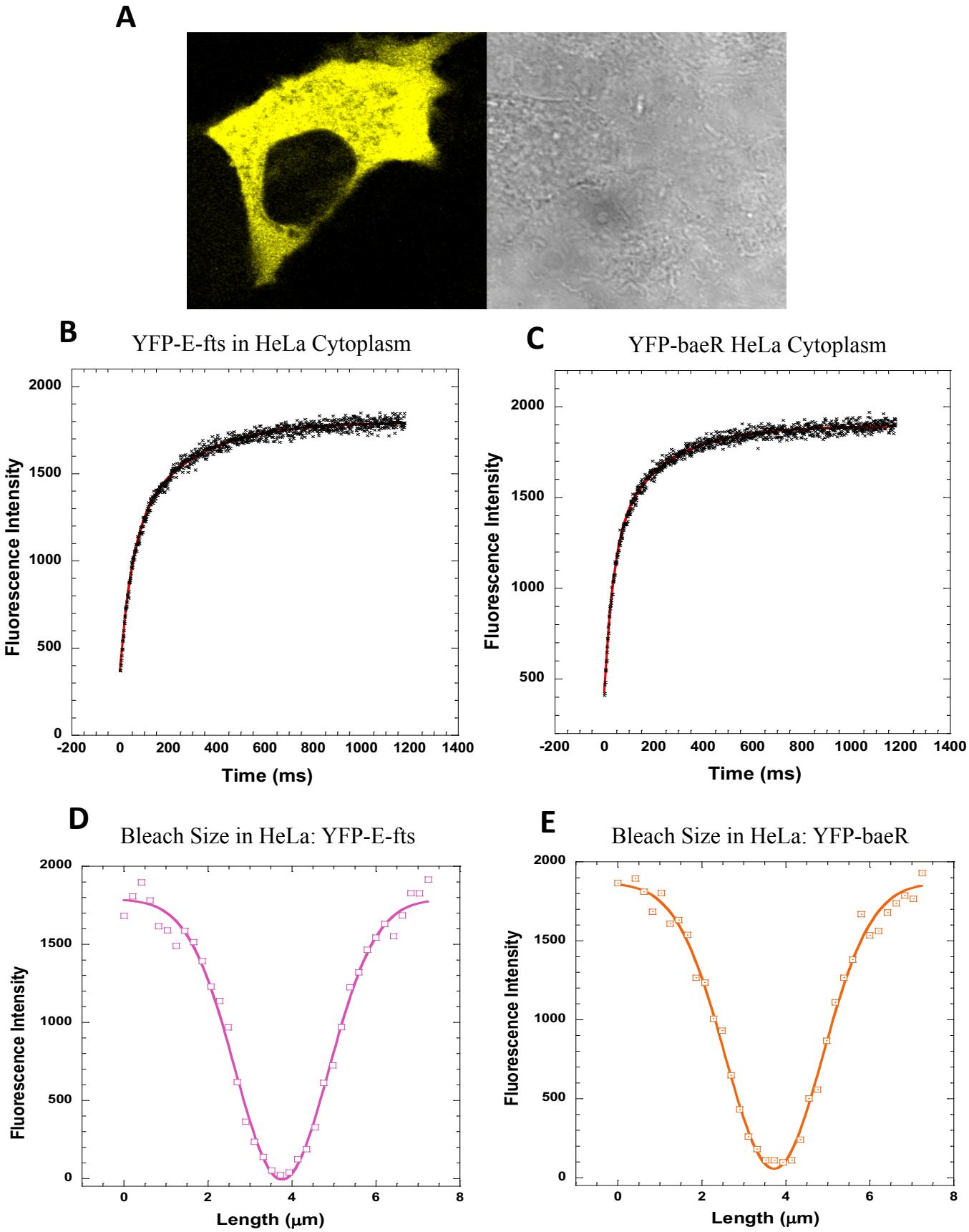

Figure 6: (A) A typical HeLa cell after successful micro-injection with a fluorescent labeled E-fts protein. (B-C): FRAP recovery profiles of (B) E-fts fused with YFP (N=43; R=0.99) (C) baeR fused with YFP (N=42; R=0.99) in HeLa cell cytoplasm. (D-E): Gaussian fits of averaged post-bleach size profiles for (D) E-fts fused with YFP (N=29; R=0.99) (E) baeR fused with YFP (N=36; R=0.99) in HeLa cell cytoplasm.

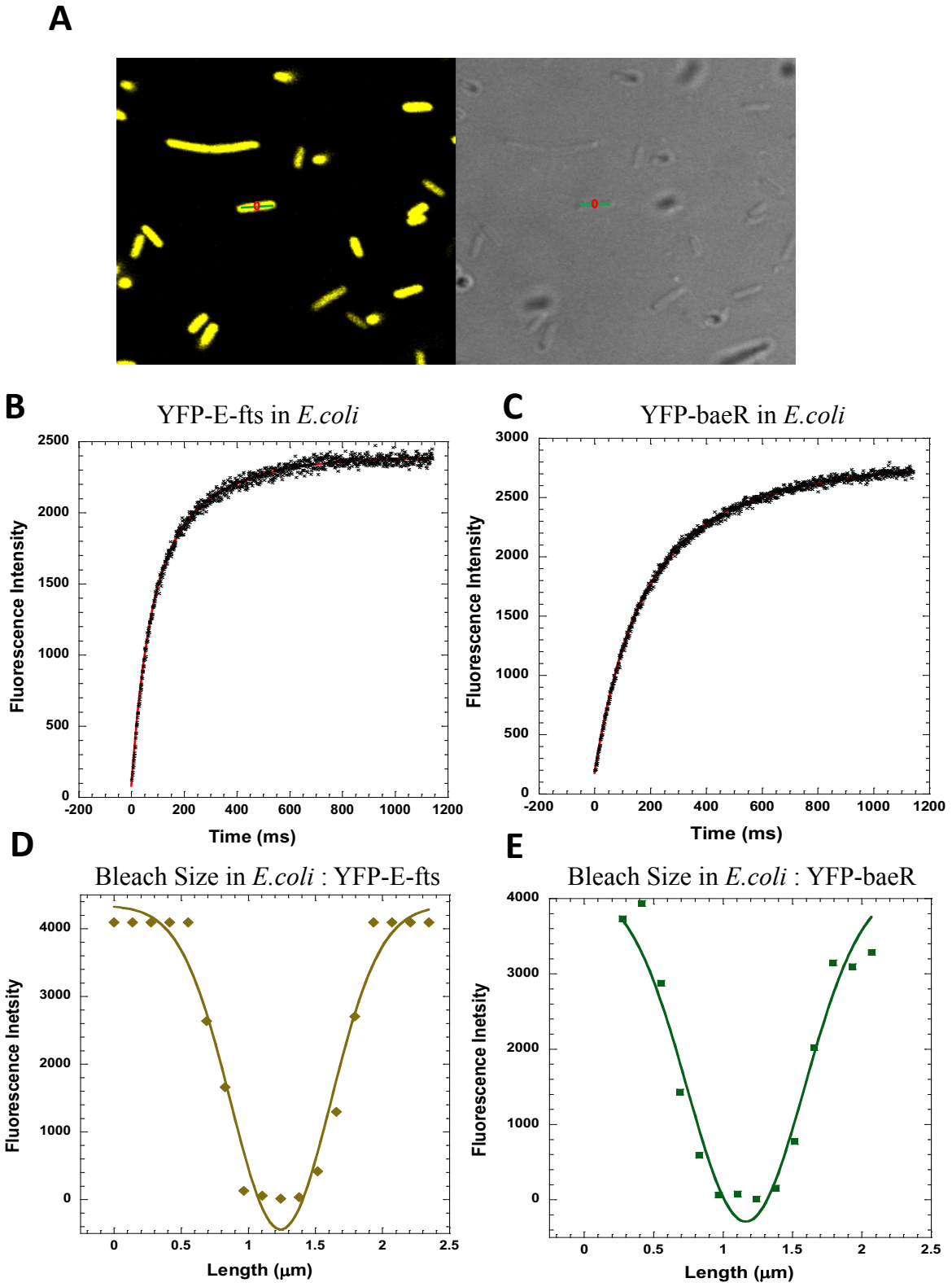

Figure 7: (A) Typical *E.Coli* cells after expression of YFP fused E-fts protein. (B, C): FRAP recovery profiles of (B) E-fts fused with YFP (N=49; R=0.99) (C) baeR fused with YFP (N=52; R=0.99) in *E.coli* cytoplasm. (D, E): Gaussian fits of post bleach size profiles for (D) E-fts fused with YFP (R= 0.98) (E) baeR fused with YFP (R= 0.97) in *E.coli* cytoplasm.

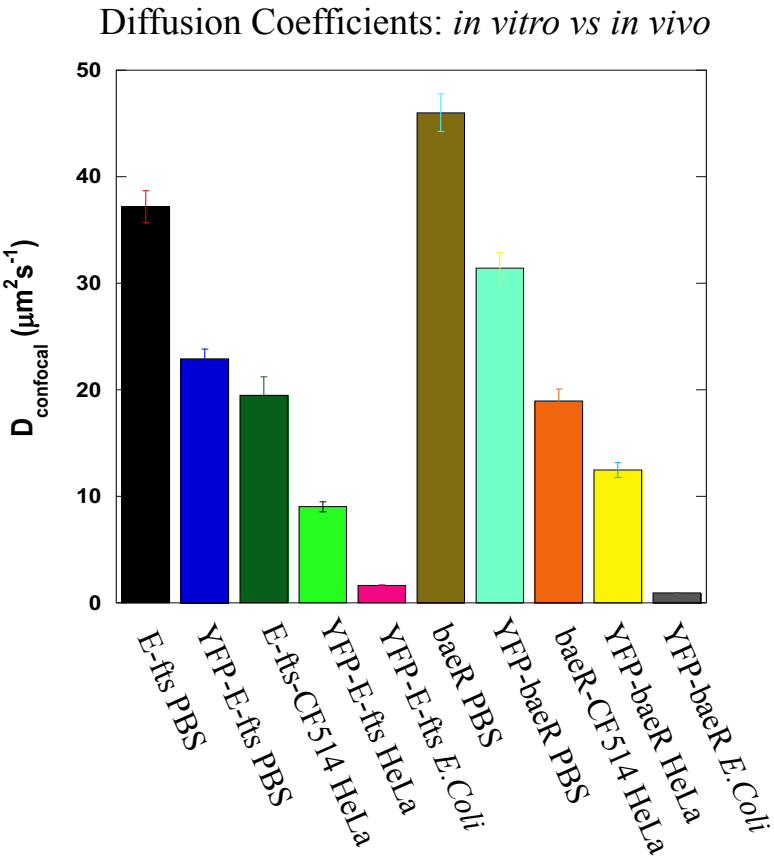

Figure 8: Comparing diffusion coefficients of E-fts and baeR proteins chemically labeled or fused with YFP in PBS buffer, HeLa cell cytoplasm and *E.coli* bacteria cells. (Final error bars are calculated after combining all the individual errors from the respective average fits).

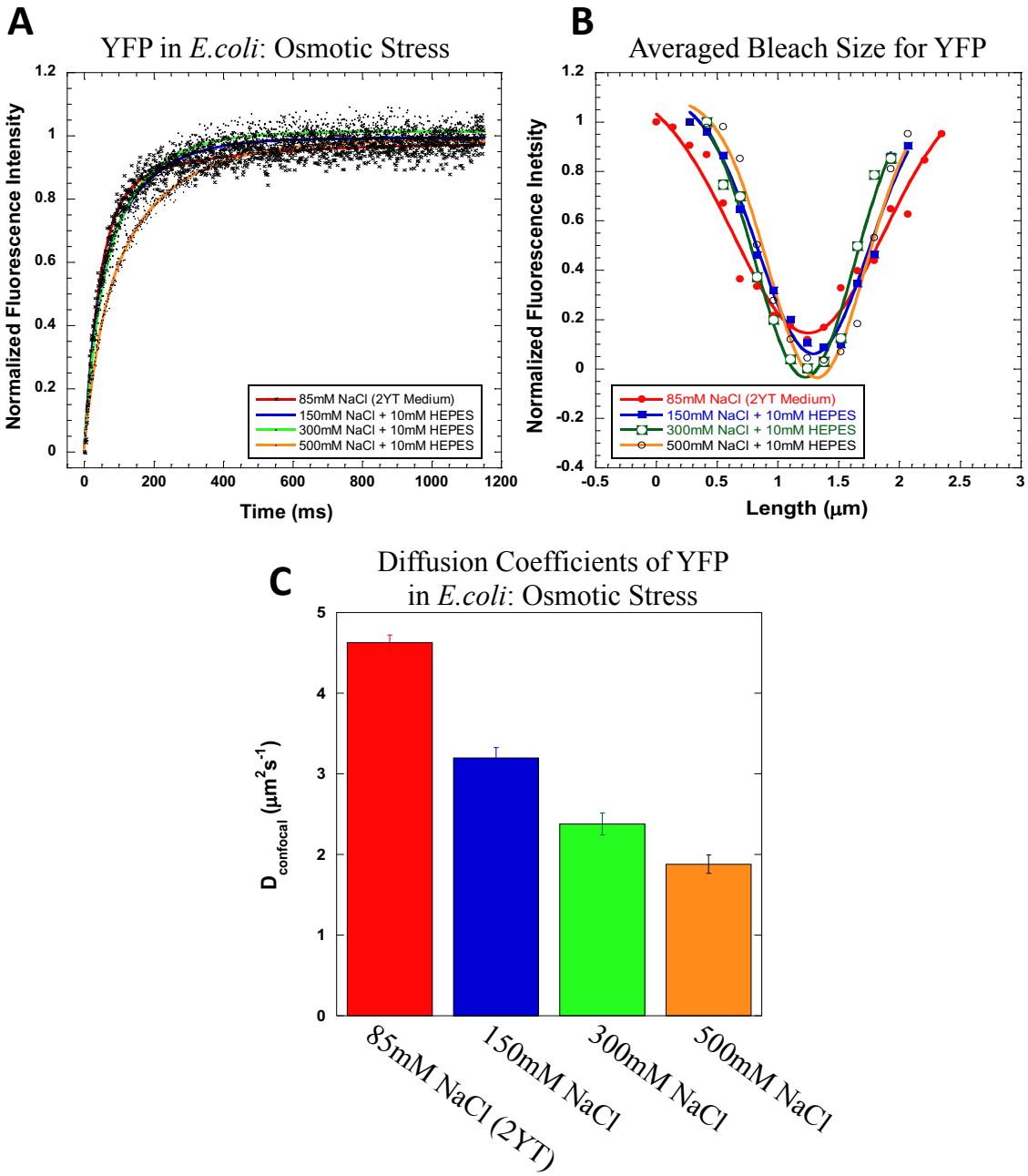

Figure 9: (A) Normalized FRAP recovery profiles (N=20;R=0.97 for YFP in 2YT, N=30;R=0.98 in 150mM, N=30;R=0.99 in 300mM and N=30;R=0.99 in 500mM NaCl) (B) corresponding Gaussian fits of averaged post-bleach size profiles (R=0.98 for YFP in 2YT, R=0.99 for 150mM, 300mM and 500mM NaCl) and (C) Comparison of diffusion coefficients for YFP protein expressed in *E.coli* cells under different osmotic stress environments (Final error bars are calculated after combining all the individual errors from the respective average fits).

.

Supporting Information

Line-FRAP, a versatile method based on fluorescence recovery after photobleaching to measure diffusion rates *in vitro* and *in vivo*

Debabrata Dey, Shir Marciano and Gideon Schreiber

Department of Biomolecular Sciences, Weizmann Institute of Science

gideon.schreiber@weizmann.ac.il

Table S1: Comparison of Line-FRAP with other Fluorescence microscopy techniques for measuring diffusion rates of Proteins in buffer and living cells

Techniques	Principle	Necessary Requirements	Sensitivity	Pros/Cons
FCS	Auto-correlation of fluorescence fluctuations	Low fluorophore concentration with high quantum yield	Not sensitive to mild and uniform bleaching	Works mainly in ideal solution condition (Gold standard) but blind towards immobile fraction if any
RICS	combination of the temporal scales of single point FCS with the spatial information obtained from ICS	Similar to FCS	Pixel size is an important consideration in designing an experiment	Indirectly measure binding by detecting changes in the diffusion coefficients *in vivo* (multiple phenomenon detections possible within a cell). Limited towards the processes that are very slow (i.e., seconds timescale) and thus cannot show correlation between pixels of one frame
SPT	Localization of a fluorescent molecule is traced over time	Low fluorophore concentrations	Sensitive to photo-bleaching and blinking	Discriminate between normal and anomalous diffusion. Auto fluorescence from the background can interfere with the measuring process.
FSM	Trajectories of co-localized fluorophore cluster inside macromolecular structures	Stable speckle formation is necessary. Primarily used to investigate the dynamics of polymers.	Less sensitive to photo-bleaching and blinking than SPT	Similar to SPT but not suitable for studying rapidly moving monomeric proteins as they do not form stable speckles.
PIPE	Spreading of initially localized photo-converted fluorophores	Photo-convertible fluorophores	Not sensitive to mild and uniform bleaching	can measure rapidly moving proteins in cytoplasm even at high concentrations
FRAP	Recovery of averaged fluorescence signal in photo-bleached region	Calibration of beam width, High concentration of fluorophores	Sensitive to reversible Photo-bleaching, bleach pulse operating time scale	Easy to perform and analysis in conventional LSMs but Limited towards the fast moving molecules especially *in vitro* condition.
FDAP/FLAC	Decay of average fluorescence signal after photo activation by a focused laser flash	Photo-convertible fluorophores, calibration of beam width same as FRAP	Sensitive to photo-bleaching	FDAP can be complementary to FRAP study
LINE-FRAP	Recovery of averaged fluorescence through a single line (along a pixel) in photo-bleached region	Two simultaneous scanners, very short bleaching point/area	Sensitive to reversible photo-bleaching, bleach time scale, bleach size area	Capable of measuring diffusion rates in solution, Eukaryotic, and Prokaryotic

RICS= Raster image correlation spectroscopy; FSM= fluorescence speckle microscopy; FLAC= Fluorescence loss after photo-conversion; FDAP=Fluorescence decay after photo-conversion;

Table S2: Diffusion Coefficients calculated from classical XY-FRAP data for labelled BSA in PBS buffer at different bleach time durations with variations in frame acquisition speed

Frame Rate	Bleach Pulse durations	k_1 ms^{-1}	k_2 ms^{-1}	a_1	a_2	p_1	p_2	τ_1	τ_2	$\tau_{1/2}$ (ave)	c_n µm	r_n µm	c_e µm	r_e µm	$D_{confocal}$ $\mu m^2 s^{-1}$
72 X 72 Pixel (14.90 µm X 14.90 µm)	63 ms	0.011	0.001	212.5	104	0.67	0.33	0.063	0.693	0.0898	0.92	1.27	4.42	3.20	29.4
36 X 36 Pixel (7.45 µm X 7.45 µm)	63 ms	0.031	0.003	612.5	169	0.78	0.22	0.022	0.231	0.0278	0.92	1.27	4.28	3.10	89.6
36 X 36 Pixel (7.45 µm X 7.45 µm)	10 ms	0.039	1×10^{-5}	799	790	0.50	0.50	0.018	69.3	0.035	0.54	0.74	2.35	1.70	21.4

The rate constants (*k*) and amplitudes (a) are from the double-exponential fit of the FRAP data. The *c* values were obtained from Gaussian fits using equation 5. The respective radius (r) are calculated assuming the respective bleach circles diameter lies at 60% height from the bottom of the Gaussian Profiles (r=1.38**c*).

Table S3: Diffusion Coefficients calculated from FRAP data for labelled BSA in PBS buffer in the presence of PEG8000 as Crowder

Bleach Pulses	% PEG 8000	η/η_0	k_1 ms^{-1}	k_2 ms^{-1}	a_1	a_2	p_1	p_2	τ_1	τ_2	$\tau_{1/2}$ (ave)	c_n µm	r_n µm	c_e µm	r_e µm	$D_{confocal}$ $\mu m^2 s^{-1}$
10 ms	5	3.0	0.082	0.006	940	285	0.77	0.23	0.0085	0.12	0.011	0.54	0.75	1.15	1.59	35.7
	10	5.0	0.069	0.007	852	324	0.72	0.28	0.010	0.10	0.013	0.54	0.75	1.15	1.59	28.8
	15	7.80	0.057	0.006	900	426	0.68	0.32	0.012	0.12	0.017	0.54	0.75	1.15	1.59	22.5
	20	12.30	0.048	0.005	801	401	0.67	0.33	0.014	0.14	0.021	0.54	0.75	1.15	1.59	18.7
63 ms	5	3.0	0.033	0.004	820	479	0.63	0.37	0.021	0.16	0.031	0.92	1.27	1.75	2.45	30.8
	10	5.0	0.028	0.004	1210	835	0.59	0.40	0.025	0.18	0.038	0.92	1.27	1.75	2.45	24.9
	15	7.80	0.025	0.003	860	649	0.57	0.43	0.028	0.20	0.045	0.92	1.27	1.75	2.45	21.3
	20	12.30	0.022	0.003	769	597	0.56	0.44	0.032	0.24	0.051	0.92	1.27	1.75	2.45	18.7

The rate constants (*k*) and amplitudes (a) are from the double-exponential fit of the FRAP data. The *c* values were obtained from Gaussian fits using equation 5. The respective radius (r) are calculated assuming the respective bleach circles diameter lies at 60% height from the bottom of the Gaussian Profiles (r=1.38**c*). Viscosity of Water (η_0) is considered as 1, for calculation of relative viscosity (η/η_0).

Table S4: Diffusion Coefficients calculated from FRAP data for different labelled proteins in different environments

Proteins	Environment	k_1 ms^{-1}	k_2 ms^{-1}	a_1	a_2	p_1	p_2	τ_1	τ_2	$\tau_{1/2}$ (ave)	c_n µm	r_n µm	c_e µm	r_e µm	$D_{confocal}$ $\mu m^2 s^{-1}$
E-fts	PBS labeled with CF514 Dye	0.041	0.005	887	482	0.65	0.35	0.017	0.14	0.024	0.92	1.27	1.73	2.38	37.2
	PBS fused with YFP	0.032	0.005	780	493	0.61	0.39	0.022	0.14	0.032	0.92	1.27	1.50	2.07	22.9
	HeLa Cytoplasm labeled with CF514 Dye	0.030	0.004	880	611	0.59	0.41	0.023	0.17	0.036	0.92	1.27	1.45	2.00	19.5
	HeLa Cytoplasm fused with YFP	0.020	0.004	753	674	0.53	0.47	0.035	0.17	0.056	0.92	1.27	1.13	1.55	9.0
	E.coli fused with YFP	0.017	0.004	1294	1018	0.56	0.44	0.042	0.17	0.063	0.54	0.75	0.38	0.52	1.6
baeR	PBS labeled with CF514 Dye	0.051	0.006	786	431	0.65	0.36	0.014	0.12	0.020	0.92	1.27	1.73	2.38	46.0
	PBS fused with YFP	0.041	0.006	985	469	0.68	0.32	0.017	0.13	0.023	0.92	1.27	1.5	2.07	31.4
	HeLa Cytoplasm labeled with CF514 Dye	0.028	0.004	468	295	0.61	0.39	0.025	0.17	0.037	0.92	1.27	1.45	2.00	19.0
	HeLa Cytoplasm fused with YFP	0.026	0.005	835	632	0.57	0.43	0.027	0.15	0.041	0.92	1.27	1.15	1.59	12.5
	E.coli fused with YFP	0.009	0.003	1246	1368	0.48	0.52	0.077	0.23	0.12	0.54	0.75	0.43	0.59	0.95
YFP	*E.coli*	0.023	0.004	1392	284	0.83	0.17	0.03	0.17	0.035	0.54	0.75	0.63	0.86	4.6

The rate constants (*k*) and amplitudes (a) are from the double-exponential fit of the FRAP data. The *c* values were obtained from Gaussian fits using equation 5. The respective radius (r) are calculated assuming the respective bleach circles diameter lies at 60% height from the bottom of the Gaussian Profiles (r=1.38**c*).

Table S5: Diffusion Coefficients of YFP protein in *E.coli* cytoplasm under Osmotic Stress Environment

NaCl Conc. (Environment)	k_1 ms^{-1}	k_2 ms^{-1}	a_1	a_2	p_1	p_2	τ_1	τ_2	$\tau_{1/2}$ (ave)	c_n µm	r_n µm	c_e µm	r_e µm	$D_{confocal}$ $\mu m^2 s^{-1}$
85mM (2YT Medium)	0.023	1392	0.004	284	0.83	0.17	0.03	0.17	0.035	0.54	0.75	0.63	0.86	4.63
150mM (10mM HEPES)	0.033	642	0.008	853	0.43	0.57	0.02	0.087	0.037	0.54	0.75	0.46	0.62	3.20
300mM (10mM HEPES)	0.025	590	0.008	738	0.44	0.56	0.03	0.091	0.045	0.54	0.75	0.40	0.55	2.38
500mM (10mM HEPES)	0.023	590	0.006	972	0.38	0.62	0.03	0.126	0.057	0.54	0.75	0.40	0.55	1.87

The rate constants (*k*) and amplitudes (a) are from the double-exponential fit of the FRAP data. The *c* values were obtained from Gaussian fits using equation 5. The respective radius (r) are calculated assuming the respective bleach circles diameter lies at 60% height from the bottom of the Gaussian Profiles (r=1.38**c*).

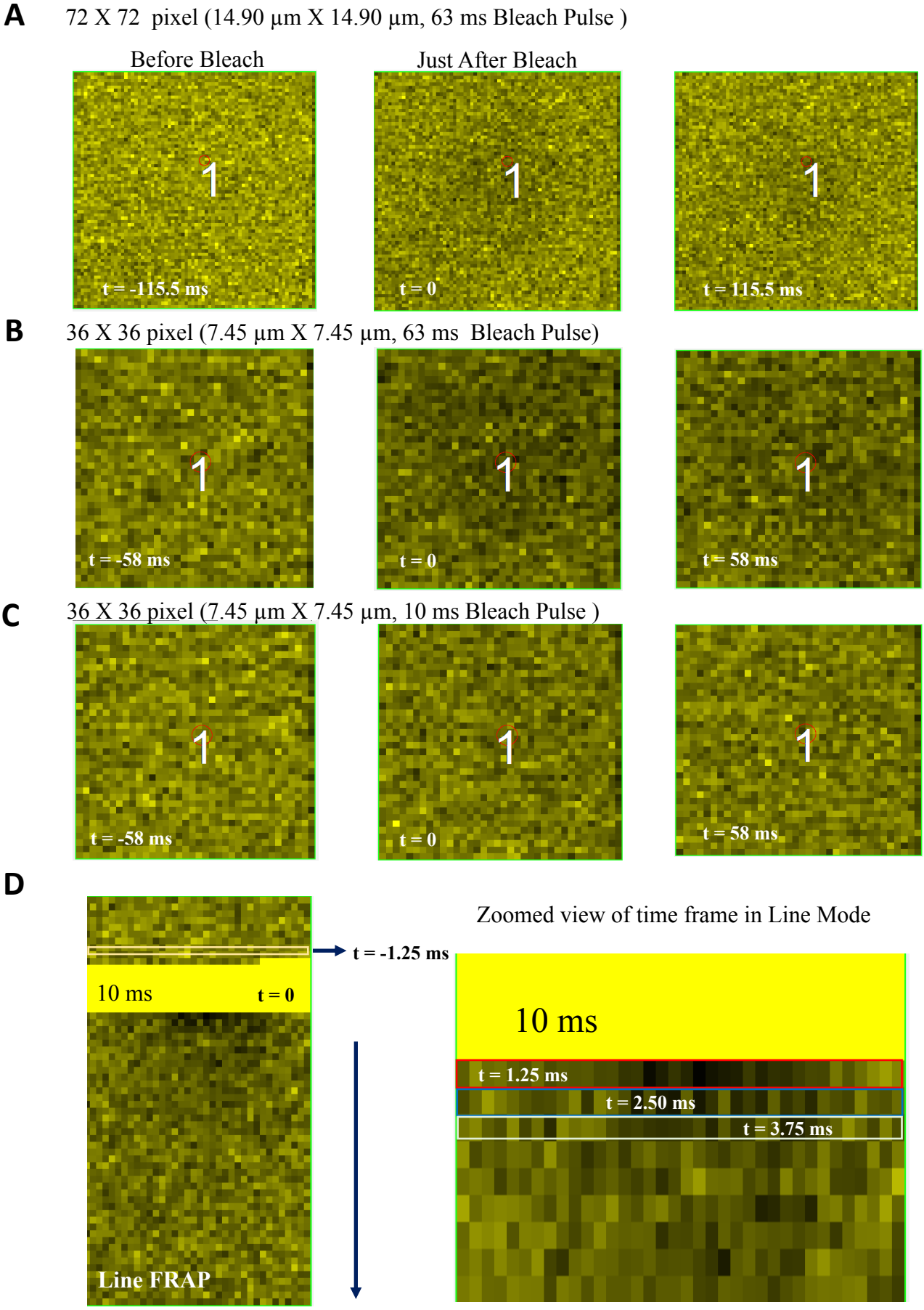

Figure S1: Acquisition of different Frame rates on fast diffusive molecule (BSA labeled with CF514 Dye in PBS buffer solution). Classical XY FRAP (A) 72X72 pixel (14.90 µm X 14.90 µm with 63 ms bleach pulse); (B) 36X36 pixel size (7.45 µm X 7.45 µm with 63 ms bleach pulse) and (C) with 10 ms bleach pulse; (D) Line FRAP with 1.25 ms time frame.

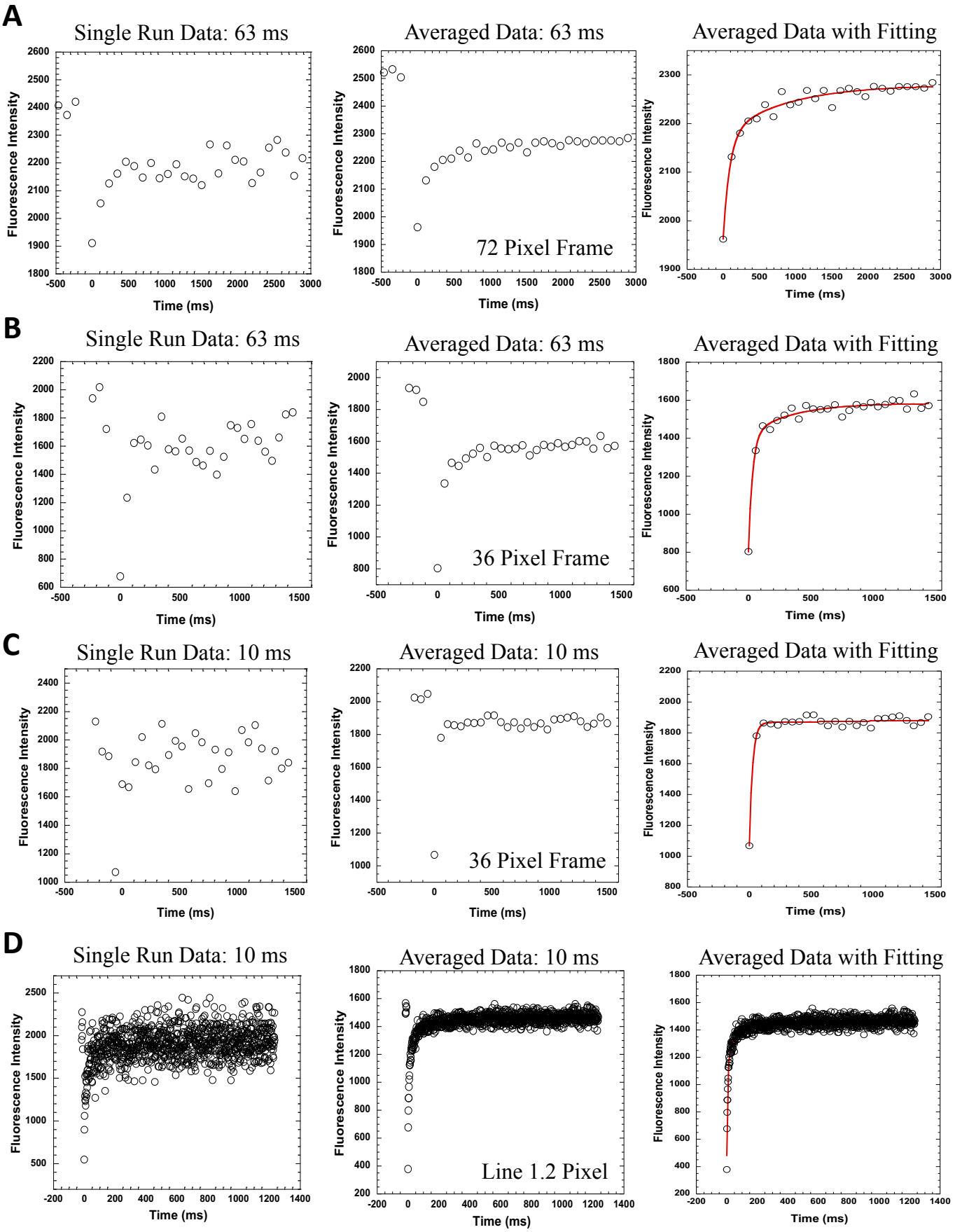

Figure S2: Effect of different frame rates on acquired recovery rate data quality in case of a faster diffusive molecule (BSA labeled with CF514 Dye in PBS buffer solution). Classical XY FRAP (A) 72X72 pixel (14.90 µm X 14.90 µm with 63 ms bleach pulse); (B) 36X36 pixel size (7.45 µm X 7.45 µm with 63 ms bleach pulse) and (C) with 10 ms bleach pulse; (D) Line FRAP with 1.25 ms time frame. Comparison of single run data vs averaged data (N=20) with their exponential fits are also shown in each cases.

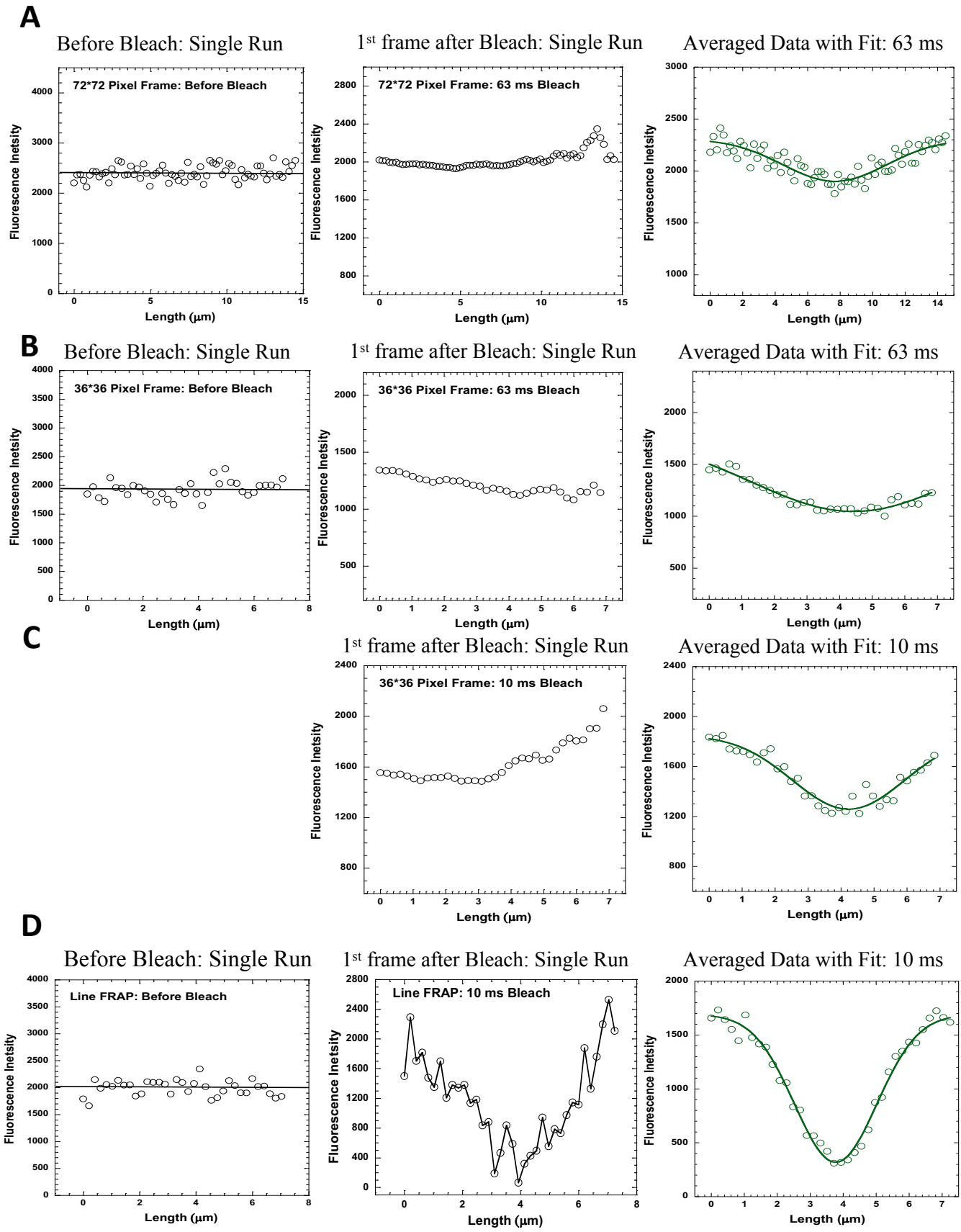

Figure S3: Effect of different frame rates on acquired bleach size data quality in case of a faster diffusive molecule (BSA labeled with CF514 Dye in PBS buffer solution). Classical XY FRAP (A) 72X72 pixel (14.90 μm X 14.90 μm with 63 ms bleach pulse); (B) 36X36 pixel size (7.45 μm X 7.45 μm with 63 ms bleach pulse) and (C) with 10 ms bleach pulse; (D) Line FRAP with 1.25 ms time frame. Comparison of single run data vs averaged data with Gaussian fitting (N=20) are also shown in each cases.

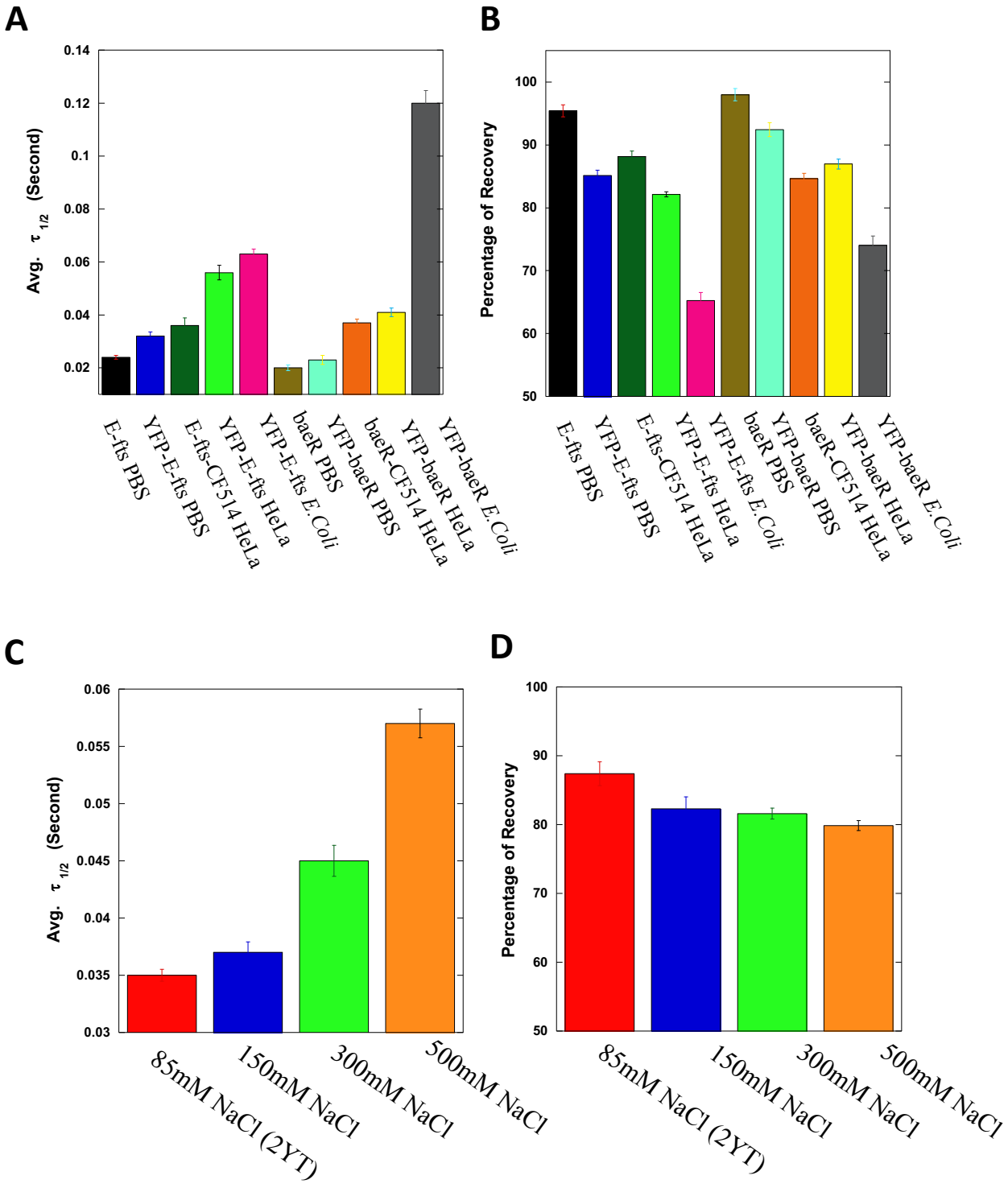

Figure S4: Comparison of (A) half-time (B) percentage of recoveries of E-fts and baeR proteins chemically labeled or fused with YFP in PBS buffer, HeLa cell cytoplasm or E.coli bacteria cells. (C) half-times (D) percentage of recoveries for YFP protein expressed in *E.coli* cells under different osmotic stress conditions.

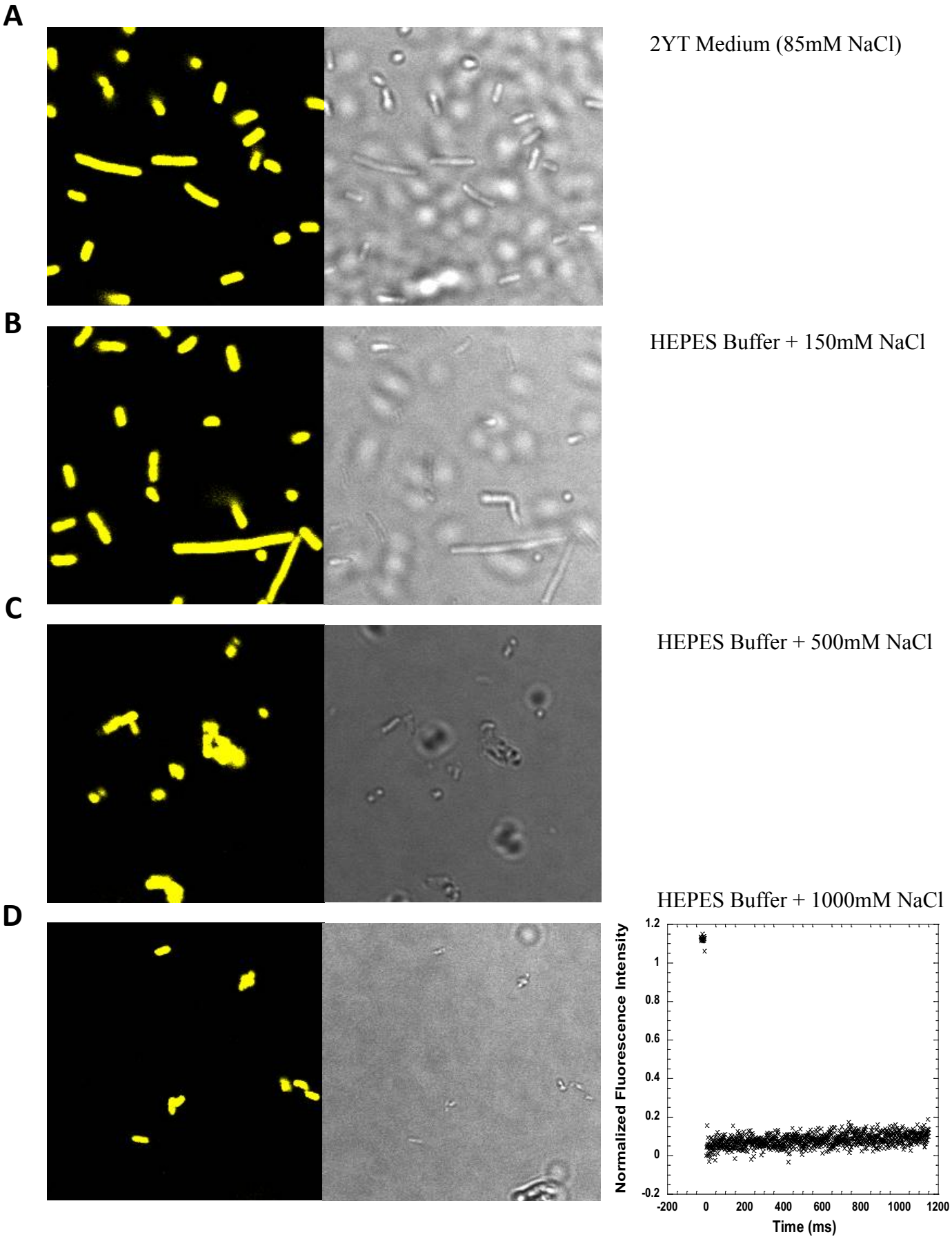

Figure S5: Visuals of *E.coli* cells under osmotically challenging environments. (A) 2YT medium (85 mM NaCl), (B) HEPES buffer + 150 mM NaCl, (C) HEPES buffer + 500 mM NaCl, (D) HEPES buffer + 1000 mM NaCl, where no fluorescence recovery was observed.